

PROCEEDINGS A

rspa.royalsocietypublishing.org

Review



Article submitted to journal

Subject Areas:Fluid Mechanics, Applied
Mathematics**Keywords:**Navier-Stokes equation, singularity
formation, extreme behavior,
energy-type estimates, numerical
optimization**Author for correspondence:**

Bartosz Protas

e-mail: bprotas@mcmaster.caSystematic Search For
Extreme and Singular
Behavior in Some
Fundamental Models of Fluid
MechanicsB. Protas¹¹Department of Mathematics and Statistics, McMaster
University, Hamilton, ON, Canada

This review article offers a survey of the research program focused on a systematic computational search for extreme and potentially singular behavior in hydrodynamic models motivated by open questions concerning the possibility of a finite-time blow-up in the solutions of the Navier-Stokes system. Inspired by the seminal work of Lu & Doering (2008), we sought such extreme behavior by solving PDE optimization problems with objective functionals chosen based on certain conditional regularity results and a priori estimates available for different models. No evidence for singularity formation was found in extreme Navier-Stokes flows constructed in this manner in 3D. We also discuss the results obtained for 1D Burgers and 2D Navier-Stokes systems, and while singularities are ruled out in these flows, the results presented provide interesting insights about sharpness of different energy-type estimates known for these systems. Connections to other bounding techniques are also briefly discussed.

1. Introduction

One of the central problems in mathematical fluid mechanics is the question whether the Navier-Stokes system, which is the main mathematical model used to describe the motion of viscous incompressible fluids, admits unique classical solutions existing globally in time for all sufficiently regular initial data [1,2]. In other words, the question is whether starting from such smooth initial data it may be possible for a “singularity” to form spontaneously in the solution such that the equations would no longer be satisfied in the classical pointwise sense. Should such situation indeed occur, this would

invalidate the Navier-Stokes system as an acceptable model to describe flows of viscous incompressible fluids. While for Navier-Stokes flows in two dimensions (2D) the problem is solved and finite-time blow-up has been ruled out [3], in the physically more relevant case of three-dimensional (3D) flows the problem remains open. Recognizing the difficulty and significance of this problem, the Clay Mathematics Institute named it one of its seven “millennium problems” posed as challenges to the mathematical community at the beginning of the 21st century [4]. On the other hand, weak solutions, which may in principle be nonunique and involve singularities, are known to exist globally in time since the work of Leray [5] and nonuniqueness was recently established in [6] for weak solutions of a certain type. Analogous questions concerning existence of unique smooth solutions also remain open for the inviscid Euler equation in 3D [7].

When fundamental properties of its solutions are studied, the Navier-Stokes system is usually considered on domains without solid boundaries, namely, the unbounded domain $\Omega = \mathbb{R}^3$ or a periodic box (3D torus) $\Omega = \mathbb{T}_L^3 := [0, L]^3$, where $L > 0$ is the domain size, and here we will focus on the latter case. Assuming we are interested in solutions on the time interval $[0, T]$, the Navier-Stokes system is defined as

$$\partial_t \mathbf{u} + \mathbf{u} \cdot \nabla \mathbf{u} + \nabla p - \nu \Delta \mathbf{u} = 0 \quad \text{in } \Omega \times (0, T], \quad (1.1a)$$

$$\nabla \cdot \mathbf{u} = 0 \quad \text{in } \Omega \times [0, T], \quad (1.1b)$$

$$\mathbf{u}(0) = \mathbf{u}_0, \quad (1.1c)$$

where $\mathbf{u} : [0, T] \times \Omega \rightarrow \mathbb{R}^3$ and $p : [0, T] \times \Omega \rightarrow \mathbb{R}$ are the velocity and pressure fields, $\nu > 0$ is the coefficient of kinematic viscosity, \mathbf{u}_0 is a divergence-free initial condition whereas the fluid density ρ is assumed constant and equal to unity ($\rho \equiv 1$). Without loss of generality, we will assume the initial data \mathbf{u}_0 to have zero mean.

In system (1.1) there are three physical parameters: the domain size L , kinetic viscosity ν and the “magnitude” of the initial data \mathbf{u}_0 . They can be combined into a single dimensionless quantity, the Reynolds number, meaning that only one of these parameters needs to be changed in order to study solutions of (1.1) in different regimes. In the investigations surveyed here one typically considers variations of the size of the initial data \mathbf{u}_0 while fixing L and ν . Thus, in keeping with these earlier studies, we will henceforth set $L = 1$ and define $\mathbb{T} := \mathbb{T}_1$, however, explicit dependence on ν will be retained in some of the estimates.

Important quantities characterizing solutions of system (1.1) include the Lebesgue norms of the velocity field

$$\|\mathbf{u}(t)\|_{L^q(\Omega)} := \left(\int_{\Omega} |\mathbf{u}(t, \mathbf{x})|^q d\mathbf{x} \right)^{\frac{1}{q}}, \quad q \geq 1, \quad (1.2)$$

as well as the kinetic energy and enstrophy¹ defined as

$$\mathcal{K}(\mathbf{u}(t)) := \frac{1}{2} \|\mathbf{u}(t)\|_{L^2(\Omega)}^2, \quad (1.3a)$$

$$\mathcal{E}(\mathbf{u}(t)) := \frac{1}{2} \int_{\Omega} |\boldsymbol{\omega}(t, \mathbf{x})|^2 d\mathbf{x} = \frac{1}{2} \|\nabla \mathbf{u}(t)\|_{L^2(\Omega)}^2, \quad (1.3b)$$

where $\boldsymbol{\omega}(t, \mathbf{x}) := \nabla \times \mathbf{u}(t, \mathbf{x})$ is the vorticity (“:=” means “equal to by definition”). In addition, we will also use Sobolev spaces $H^s(\Omega)$, $s \in \mathbb{R}^+$, of functions with square-integrable weak derivatives of order s [14].

The question about the possibility of singularity formation in solutions of the Navier-Stokes system (1.1) is primarily a problems in mathematical analysis of partial differential equations (PDEs). An important class of results obtained to date has the form of “conditional regularity results” stating conditions which need to be satisfied by a Leray-Hopf weak solution for it to also satisfy system (1.1) in the classical sense, i.e., pointwise in $(0, T] \times \Omega$. Typically, such solutions

¹We note that unlike energy, cf. (1.3a), enstrophy is often defined without the factor of 1/2. However, for consistency with earlier studies belonging to this research program [8–13], we choose to retain this factor here.

will then also be smooth (real-analytic) [15]. Conditional regularity results are often accompanied by a priori estimates involving some related quantities and also applicable to weak solutions. Arguably, the best known conditional regularity result is the enstrophy condition [16] asserting that $\mathbf{u}(t)$ is a smooth solution of system (1.1) on the time interval $[0, T]$ provided its enstrophy (1.3b) remains bounded, i.e.,

$$\sup_{0 \leq t \leq T} \mathcal{E}(\mathbf{u}(t)) < \infty. \quad (1.4)$$

While it is not known whether (1.4) is true for all initial data \mathbf{u}_0 and arbitrarily large T , Leray-Hopf weak solutions satisfy $\int_0^T \mathcal{E}(\mathbf{u}(t)) dt < \infty$ (however, the boundedness of $\int_0^T \mathcal{E}(\mathbf{u}(t))^2 dt$ is an open question).

Another important conditional regularity result is given by the family of the Ladyzhenskaya-Prodi-Serrin conditions asserting that Navier-Stokes flows $\mathbf{u}(t)$ are smooth and satisfy system (1.1) in the classical sense provided that [17–19]

$$\mathbf{u} \in L^p([0, T]; L^q(\Omega)), \quad 2/p + 3/q = 1, \quad q > 3. \quad (1.5)$$

These conditions were recently generalized in [20] to include norms of the derivatives of the velocity field. As regards the limiting case with $q = 3$, the corresponding condition was established in [21]

$$\mathbf{u} \in L^\infty([0, T]; L^3(\Omega)) \quad (1.6)$$

and a related blow-up criterion was recently obtained in [22]. Condition (1.5) implies that should a singularity form in a classical solution $\mathbf{u}(t)$ of the Navier-Stokes system (1.1) at some finite time $0 < t_0 < \infty$, then necessarily

$$\lim_{t \rightarrow t_0} \int_0^t \|\mathbf{u}(\tau)\|_{L^q(\Omega)}^p d\tau \rightarrow \infty, \quad 2/p + 3/q = 1, \quad q > 3. \quad (1.7)$$

At the same time, the time evolution of the solution norm $\|\mathbf{u}(t)\|_{L^q(\Omega)}$ on the time interval $[0, T]$ is subject to the some a priori bounds valid also for Leray-Hopf weak solutions [20], which might involve singularities. An estimate of this type was discussed in [23] and was rederived with an upper bound explicitly depending on the initial data in [24]

$$\int_0^T \|\mathbf{u}(\tau)\|_{L^q(\Omega)}^{\frac{4q}{3(q-2)}} d\tau \leq C \mathcal{K}_0^{\frac{2q}{3(q-2)}}, \quad 2 \leq q \leq 6, \quad (1.8)$$

where $\mathcal{K}_0 := \mathcal{K}(\mathbf{u}_0)$ and $C > 0$ is a generic constant whose numerical value may vary between different estimates. We note that the integrals in (1.7) and (1.8) differ in the exponent in the integrand expressions which is smaller in the latter case.

We add that in the context of the inviscid Euler system a conditional regularity result analogous to (1.4) and (1.5)–(1.6) is given by the Beale-Kato-Majda (BKM) criterion which asserts that an Euler flow remains smooth on $[0, T]$ if and only if $\int_0^T \|\boldsymbol{\omega}(\tau)\|_{L^\infty(\Omega)} d\tau < \infty$ [25]. A relation between potential blow-up in Euler flows and Navier-Stokes flows with sufficiently small viscosity was established in [26]. Recently, finite-time singularity formation in 3D axisymmetric Euler flows on domains exterior to a boundary with conical shape was proved in [27].

In order to obtain insights about the enstrophy condition (1.4), we assume the Navier-Stokes system (1.1) admits a smooth classical solution $\mathbf{u}(t)$ for times $t \in [0, T]$, where T is sufficiently small, which is guaranteed by local existence theorems [15]. We then consider the equations for the evolution of the kinetic energy (1.3a) and the enstrophy (1.3b) obtained multiplying (1.1a) by, respectively, \mathbf{u} and $\boldsymbol{\Delta}\mathbf{u}$, integrating over Ω and performing integrations by parts (these operations are justified for $t \in [0, T]$ since the solution $\mathbf{u}(t)$ is smooth there)

$$\frac{d\mathcal{K}(\mathbf{u}(t))}{dt} = -\nu \mathcal{E}(\mathbf{u}(t)), \quad (1.9a)$$

$$\frac{d\mathcal{E}(\mathbf{u}(t))}{dt} = -\nu \int_{\Omega} |\boldsymbol{\Delta}\mathbf{u}|^2 dx + \int_{\Omega} \mathbf{u} \cdot \nabla \mathbf{u} \cdot \boldsymbol{\Delta}\mathbf{u} dx =: \mathcal{R}_{\mathcal{E}}(\mathbf{u}). \quad (1.9b)$$

As shown in [28], relation (1.9b) can be used to obtain the following upper bound on the rate of growth of enstrophy

$$\frac{d\mathcal{E}}{dt} \leq \frac{27}{8\pi^4\nu^3}\mathcal{E}^3. \quad (1.10)$$

By simply integrating the differential inequality in (1.10) with respect to time we obtain the finite-time bound

$$\mathcal{E}(\mathbf{u}(t)) \leq \frac{\mathcal{E}_0}{\sqrt{1 - \frac{27}{4\pi^4\nu^3}\mathcal{E}_0^2 t}}, \quad (1.11)$$

where $\mathcal{E}_0 := \mathcal{E}(\mathbf{u}_0)$, which becomes infinite at time $t_0 = 4\pi^4\nu^3/(27\mathcal{E}_0^2)$. Thus, based on inequality (1.11), which is the best estimate available to date, it is not possible to establish the boundedness of the enstrophy $\mathcal{E}(\mathbf{u}(t))$ required in condition (1.4) and hence also the regularity of solutions globally in time. However, boundedness of enstrophy and existence of smooth solutions can be established for arbitrarily long times provided the initial data \mathbf{u}_0 is “small”, more precisely, when $\mathcal{K}_0\mathcal{E}_0 = \mathcal{O}(\nu^4)$ [28].

In a similar vein, the Ladyzhenskaya-Prodi-Serrin condition (1.7) can be studied by considering the rate of growth of the L^q norm of the velocity field, for which an upper bound was already known to Leray [5], see also [29–31],

$$\frac{1}{q} \frac{d}{dt} \|\mathbf{u}(t)\|_{L^q(\Omega)}^q \leq C \|\mathbf{u}(t)\|_{L^q(\Omega)}^{\frac{q(q-1)}{q-3}}, \quad q > 3. \quad (1.12)$$

However, as was the case with the enstrophy condition, this approach does not lead to estimates that would allow one to ascertain the finiteness of the integral expression in (1.7).

While the blow-up problem is fundamentally a question in mathematical analysis, a lot of computational studies have been carried out since the mid-’80s in order to shed light on the hydrodynamic mechanisms which might lead to singularity formation in finite time. Given that such flows evolving near the edge of regularity involve formation of very small flow structures, these computations typically require the use of state-of-the-art computational resources available at a given time. The computational studies focused on the possibility of finite-time blow-up in the 3D Navier-Stokes and/or Euler system include [7,32–45], all of which considered problems defined on domains periodic in all three dimensions. The investigations [46–49] focused on the time evolution of vorticity moments and compared it against bounds on these quantities obtained using rigorous analysis. Recent computations [50] considered a “trefoil” configuration meant to be defined on an unbounded domain (although the computational domain was always truncated to a finite periodic box). A simplified semi-analytic model of vortex reconnection was recently developed and analyzed based on the Biot-Savart law and asymptotic techniques [51,52]. We also mention the studies [53] and [54], along with references found therein, in which various complexified forms of the Euler equation were investigated. The idea of this approach is that, since the solutions to complexified equations have singularities in the complex plane, singularity formation in the real-valued problem is manifested by the collapse of the complex-plane singularities onto the real axis. Overall, the outcome of these investigations is rather inconclusive: while for the Navier-Stokes system most of the recent computations do not offer support for finite-time blow-up, the evidence appears split in the case of the Euler system. In particular, the studies [43] and [42] hinted at the possibility of singularity formation in finite time. In this connection we also highlight the computational investigations [55,56] in which blow-up was documented in axisymmetric Euler flows on a bounded (tubular) domain. Recently, numerical evidence for blow-up in solutions of the Navier-Stokes system in 3D axisymmetric geometry with a degenerate variable diffusion coefficient was provided in [57].

An entirely different approach designed to *systematically* search for potentially singular Navier-Stokes flows was proposed by Lu & Doering based on the conditional regularity result (1.4) in [28] and was later developed in [8,9,11–13,24]. The idea is to look for initial data which might potentially lead to a finite-time singularity as a solution of a certain variational optimization problem with the objective functional and constraints motivated by estimates (1.10)–(1.11). In

addition, in this framework it is also possible to check (usually at the level of computational evidence) the sharpness of a priori estimates such as (1.10). We say that a polynomial upper bound of the type $C\mathcal{E}^\alpha$ for some $\alpha > 0$ is sharp (up to a numerical prefactor) if the expression on the left-hand side (LHS) of the estimate is $\mathcal{O}(\mathcal{E}^\alpha)$ as $\mathcal{E} \rightarrow \infty$. A family of initial conditions and the corresponding flows parameterized by \mathcal{E}_0 and saturating a certain estimate in the above sense is referred to as “extreme”. Energy-type estimates similar to (1.10)–(1.11) are also known for the one-dimensional (1D) viscous Burgers equation and the two-dimensional (2D) Navier-Stokes system. While these two systems are known to be globally well-posed [3], the question whether these estimates are sharp is in fact quite pertinent, because they are established using similar mathematical techniques as (1.10)–(1.11). These estimates are obtained from the governing equations applying different functional inequalities and although each of these inequalities is known to be sharp, sharpness need not be preserved if they are chained together (because different inequalities are saturated by different fields).

These observations have motivated a research program focused on probing the sharpness of a number of key estimates, both instantaneous as in (1.10) and finite-time as in (1.11), in the 1D Burgers and 2D Navier-Stokes systems, in addition to examining estimates (1.10)–(1.11) and more recently the Ladyzhenskaya-Prodi-Serrin criterion (1.7) in 3D Navier-Stokes flows. Progress in this research program was largely enabled by the development of robust computational approaches for the solution of large-scale PDE-constrained optimization problems. Since a number of important milestones has recently been attained in this research program, the present review paper aims to survey these developments.

Most of the optimization problems considered here are nonconvex, hence their solutions found numerically based on local optimality conditions are local maximizers only. Thus, unless stated otherwise, when we refer to “maximizing solutions” defined with $\arg \max$ we will in fact mean local maximizers. Theoretical results concerning existence of (possibly nonunique) solutions to optimization problem involving different hydrodynamic PDE models are available in the literature, which includes the seminal study [58] and the monographs [59–61].

The structure of the paper is as follows: in the next three sections we review instantaneous and finite-time energy-type estimates known for the 1D Burgers, 2D and 3D Navier-Stokes systems, and discuss different optimization problems that have been introduced to test their sharpness before presenting some key results (in Section 2 devoted to the 1D Burgers equation we also provide comments about the corresponding stochastic problem and the system with fractional dissipation); in Section 5 we draw some connections to other research problems concerned with establishing bounds on the behavior of hydrodynamic models such as the background method and the methods based on sum-of-squares (SOS) polynomial bounds; finally, summary and conclusions are deferred to Section 6 where we also provide an outlook; more technical material concerning the numerical solution of the optimization problems studied in this research program is collected in an appendix.

2. Estimates for the 1D Burgers Equation

The 1D viscous Burgers equation

$$\partial_t u + \frac{1}{2} \partial_x u^2 - \nu \partial_{xx} u = 0 \quad \text{in } (0, T] \times \Omega, \quad (2.1a)$$

$$u(0) = u_0, \quad (2.1b)$$

where $\Omega = \mathbb{T}$ is a periodic domain and u_0 the initial condition, has often been used as a highly idealized model of the Navier-Stokes system [62]. Unlike its inviscid variant (obtained by setting $\nu = 0$ in (2.1a)) which exhibits a well-documented finite-time blow-up, system (2.1) is globally well posed in the classical sense [3]. As shown in [28], defining the 1D equivalent of enstrophy as

$$\mathcal{E}(u(t)) := \frac{1}{2} \int_0^1 |\partial_x u(t, x)|^2 dx, \quad (2.2)$$

it is possible to obtain an estimate for the rate of growth of enstrophy analogous to (1.10) in the form²

$$\frac{d\mathcal{E}}{dt} \leq 3 \left(\frac{1}{2\pi^2\nu} \right)^{1/3} \mathcal{E}^{5/3}. \quad (2.3)$$

Based on this estimate, the corresponding finite-time bound on enstrophy was obtained in [8] by integrating (2.3) in time

$$\max_{t \in [0, T]} \mathcal{E}(u(t)) \leq \left[\mathcal{E}_0^{1/3} + \frac{1}{4} \left(\frac{1}{2\pi^2\nu} \right)^{4/3} \mathcal{E}_0 \right]^3 \xrightarrow{\mathcal{E}_0 \rightarrow \infty} \frac{1}{64} \left(\frac{1}{2\pi^2\nu} \right)^4 \mathcal{E}_0^3. \quad (2.4)$$

We emphasize that in contrast to (1.11) this bound is valid uniformly in t . Moreover, it also exhibits a well-defined asymptotic behavior in the large enstrophy limit. In this context one should also mention Biryuk's work [63] which implies a finite-time bound with a smaller exponent, namely, $\max_{t \geq 0} \mathcal{E}(u(t)) \leq C_B \mathcal{E}_0^{3/2}$. While this approach did not rely on time integration of an instantaneous estimate such as (2.3), the prefactor in this estimate $C_B = C_B(\|u_0\|_{H^2})$ requires the H^2 norm of the initial data u_0 to be bounded. Consequently, owing to Poincaré's inequality, this prefactor will not remain bounded in the limit we are interested in, i.e., as $\mathcal{E}_0 \rightarrow \infty$.

Lu & Doering [28] posed an interesting question about the sharpness of estimate (2.3) and to elucidate it formulated the following optimization problem

Problem 1. Given $\mathcal{E}_0 \in \mathbb{R}_+$ and the objective functional, cf. (1.9b),

$$r(u) := -\nu \|\partial_{xx} u\|_{L^2([0,1])}^2 - \frac{1}{2} \int_0^1 (\partial_x u)^3 dx = \frac{d\mathcal{E}(u(t))}{dt}, \quad (2.5)$$

find

$$\tilde{u}_{\mathcal{E}_0} = \arg \max_{u \in \Sigma_{\mathcal{E}_0}} r(u), \quad \text{where} \quad \Sigma_{\mathcal{E}_0} := \left\{ u \in H^2(\Omega) : \int_0^1 u dx = 0, E(u) = \mathcal{E}_0 \right\}.$$

The idea behind this problem is to maximize the LHS in estimate (2.3) for a range of values of the constraint \mathcal{E}_0 to see whether the maximum attainable values of $d\mathcal{E}/dt$, cf. (2.5), saturate the upper bound on the RHS, in the sense of having the same dependence on \mathcal{E}_0 . Remarkably, Lu & Doering were able to solve Problem 1 in a closed form using the method of Lagrange multipliers with the optimal solution $\tilde{u}_{\mathcal{E}_0}$ expressed in terms of elliptic integrals and Jacobi elliptic functions. By analyzing the asymptotic behavior of these solutions for large enstrophies, they concluded that

$$r(\tilde{u}_{\mathcal{E}_0}) \sim \frac{0.393}{\nu^{1/3}} \mathcal{E}_0^{5/3} \quad \text{as} \quad \mathcal{E}_0 \rightarrow \infty, \quad (2.6)$$

thus demonstrating that estimate (2.3) is sharp (up to a numerical prefactor which is larger than in (2.6) by about 2.83). In other words, for each value of \mathcal{E}_0 , the optimal fields $\tilde{u}_{\mathcal{E}_0}$, which have the form of steep waves with fronts becoming sharper as \mathcal{E}_0 increases, instantaneously produce as much enstrophy $r(\tilde{u}_{\mathcal{E}_0})$ as is only allowed by the mathematically rigorous analysis of the 1D Burgers system (2.1). On the other hand, solving the Burgers system with optimizers $\tilde{u}_{\mathcal{E}_0}$ of Problem 1 used as the initial data produces maximum enstrophy which scales as $\mathcal{O}(\mathcal{E}_0)$ for large \mathcal{E}_0 , far below what is allowed by estimate (2.4).

The companion question about sharpness of the corresponding finite-time estimate (2.4) was taken up by Ayala & Protas in [8] where the following optimization problem was considered

²Due to the presence of the factor 1/2 in (2.2), the coefficients in (2.3) and (2.6) differ from those given in [28]. For the same reason, relations (4) and (5) in [8] contain incorrect prefactors. The second term on the RHS in relation (2.5) appears with an incorrect sign in [28] and in [8].

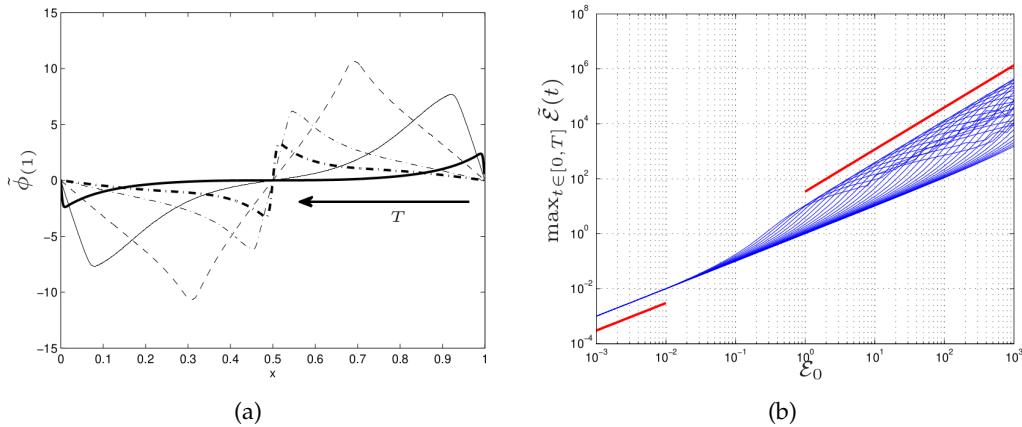


Figure 1. (a) Optimal initial conditions $\tilde{u}_{0;\mathcal{E}_0,T}$ obtained by solving Problem 2 with fixed entrophy $\mathcal{E}_0 = 10^3$ and different time intervals: (thick solid line) $T = 10^{-3}$, (thin solid line) $T = 10^{-2}$, (thin dashed line) $T = 10^{-1.5}$, (thin dotted line) $T = 10^{-1}$ and (thick dotted line) $T = 10^0$; the arrow indicates the trend with increasing T . (b) Maximum entrophy $\max_{t \in [0, T]} \mathcal{E}_T(\tilde{u}_{0;\mathcal{E}_0,T})$ as a function of initial entrophy \mathcal{E}_0 for different T . Two distinct power laws can be observed with exponents 1 for small \mathcal{E}_0 and 3/2 for large \mathcal{E}_0 , cf. (2.7).

Problem 2. Given $\mathcal{E}_0, T \in \mathbb{R}_+$ and the objective functional $\mathcal{E}_T(u_0) := \mathcal{E}(u(T))$, find

$$\tilde{u}_{0;\mathcal{E}_0,T} = \arg \max_{u_0 \in \Xi_{\mathcal{E}_0}} \mathcal{E}_T(u_0), \quad \text{where} \quad \Xi_{\mathcal{E}_0} := \left\{ u_0 \in H^1(\Omega) : \int_0^1 u_0 dx = 0, \mathcal{E}(u_0) = \mathcal{E}_0 \right\}.$$

The idea behind this problem is to find optimal initial data $\tilde{u}_{0;\mathcal{E}_0,T}$ with prescribed entrophy \mathcal{E}_0 that at the given time T produces the largest entrophy $\mathcal{E}_T(\tilde{u}_{0;\mathcal{E}_0,T})$. We emphasize that in involving the flow evolution on $[0, T]$, Problem 2 is fundamentally different, and arguably harder to solve, than Problem 1 where the instantaneous only amplification of entrophy is considered. Problem 2 was solved in [8] with $\nu = 10^{-3}$ for a broad range of values of \mathcal{E}_0 and T using the adjoint-based gradient-ascent method described in Appendix A and some results are summarized in Figures 1a and 1b. As is evident from Figure 1a, the optimal initial data $\tilde{u}_{0;\mathcal{E}_0,T}$ obtained for a fixed entrophy \mathcal{E}_0 and a short time window T features a steep front and hence resembles the instantaneous maximizers $\tilde{u}_{\mathcal{E}_0}$ found in [28] by solving Problem 1, however, as T increases it gradually turns into a rarefaction wave. By maximizing the results presented in Figure 1b with respect to T at fixed values of \mathcal{E}_0 , we obtain the relation

$$\max_T \mathcal{E}_T(\tilde{u}_{0;\mathcal{E}_0,T}) \sim 11.488 \mathcal{E}_0^{1.531} \quad \text{as} \quad \mathcal{E}_0 \rightarrow \infty, \quad (2.7)$$

where the exponent of \mathcal{E}_0 is lower, roughly by a factor of 2, than the exponent 3 in the finite-time estimate (2.4). This indicates that this estimate may not be sharp and could possibly be improved by lowering the exponent of \mathcal{E}_0 . We will return to this question in Section 5.

Properties of extreme Burgers flows corresponding to the initial data $\tilde{u}_{0;\mathcal{E}_0,T}$ obtained as local maximizers of Problem 2 were analyzed by Pelinovsky [64,65]. In particular, subject to the additional assumption that the initial condition be given in terms of an odd C^3 function, an $\mathcal{O}(\mathcal{E}_0^{3/2})$ estimate was established in [64] on the maximum growth of entrophy $\max_t \mathcal{E}(t)$, cf. (2.7). It was obtained applying Laplace's method to produce an asymptotic representation for large \mathcal{E}_0 of the solution to (2.1) given in terms of the Cole-Hopf formula. These results provide a rigorous and quantitative justification for the behavior of Burgers flows with initial data $\tilde{u}_{0;\mathcal{E}_0,T}$ obtained as local maximizers of Problem 2.

Since Problem 2 is nonconvex and the numerical approach employed to solve it relies on local optimality conditions, cf. Appendix A, we of course cannot guarantee that the solutions found for any \mathcal{E}_0 and T , cf. Figures 1a,b, are global maximizers. However, the results reported in [8] were

obtained following a thorough search involving the use of many different, mutually orthogonal (in the function space $H^1(\Omega)$), and random initial guesses $u^{(0)}$. The optimal initial conditions shown in Figure 1a are in fact nonunique maximizers as their rescaled copies $(1/m)\tilde{u}_{0;\mathcal{E}_0,T}(mx)$, $x \in [0, 1]$, $m = 2, 3, \dots$, were also found to be local maximizers, but characterized by smaller values of \mathcal{E}_T . Further support for the conjecture that at least up to a certain value of \mathcal{E}_0 the maximizers presented in Figure 1a are in fact global maximizers was provided in [66] where upper bounds on $\max_{t \geq 0} \mathcal{E}(t)$ revealing behavior consistent with (2.7) were obtained based on a Galerkin truncation of the Burgers system (2.1). We will discuss this important point in more detail in Section 5.

An intriguing question, originally raised by Flandoli [67], is how extreme or singular behavior possible in solutions of hydrodynamic models may be affected by stochastic forcing. More specifically, the question is whether via some interaction with the nonlinearity and dissipation present in the system such stochastic forcing may enhance or weaken the growth of certain solution norms as compared to the deterministic case. In particular, in the case of systems exhibiting finite-time blow-up in the deterministic setting it is interesting to know whether noise may accelerate or delay the formation of a singularity, or perhaps even prevent it entirely [67]. The question how colored additive noise in 1D Burgers equation affects the dependence of the maximum attained enstrophy $\max_{t \geq 0} \mathcal{E}(t)$ on \mathcal{E}_0 was investigated using stochastic Monte-Carlo techniques in [68]. It was shown however that the expected values of the enstrophy in stochastic Burgers flows with the optimal initial conditions $\tilde{u}_{0;\mathcal{E}_0,T}$ exhibit the same power-law dependence on the initial enstrophy \mathcal{E}_0 as in the deterministic case, cf. (2.7).

An interesting generalization of system (2.1) is the fractional Burgers system

$$\partial_t u + \frac{1}{2} \partial_x u^2 + \nu (-\Delta)^\alpha u = 0 \quad \text{in } (0, T] \times \Omega, \quad (2.8a)$$

$$u(0) = u_0, \quad (2.8b)$$

where $(-\Delta)^\alpha$, $\alpha \in [0, 1]$, is the fractional Laplacian defined for sufficiently smooth functions $v : \Omega \rightarrow \mathbb{R}$ in terms of the relation $\left[(-\Delta)^\alpha v\right]_k := |k|^{2\alpha} [\hat{v}]_k$, $k \in \mathbb{Z}$, in which $[\hat{v}]_k$ is the Fourier coefficient of v with wavenumber k . As shown in [69], system (2.8) admits globally-defined smooth classical solutions in the subcritical ($\alpha \in (1/2, 1]$) and in the critical ($\alpha = 1/2$) regime. On the other hand, finite-time blow-up occurs in the supercritical regime ($\alpha \in [0, 1/2)$). The fractional Burgers system is thus a useful simple model to study singular behavior, especially given the fact that the 3D Navier-Stokes system is also known to be globally well posed in the classical sense in the presence of fractional dissipation with exponents $\alpha \geq 5/4$ [70]. The fractional Burgers system (2.8) has also been studied in connection with turbulence [71].

Generalizations of the instantaneous estimate (2.3) for the case of the fractional Burgers system (2.8) have been obtained in [12]. It was shown that the dependence of the bounds on the enstrophy rate of growth $d\mathcal{E}/dt$ on \mathcal{E}_0 has the same global form $\sigma \mathcal{E}_0^\gamma$ in the subcritical, critical and parts of the supercritical regime with the exponent γ increasing without bound as the fractional dissipation exponent α is reduced from 1 (where $\gamma = 5/3$, cf. (2.3)) to $1/4$. Moreover, by solving numerically a variant of Problem 1, these new estimates were shown to be sharp (up to numerical prefactors). Finally, singularity formation in the supercritical regime and transient behavior in the subcritical case were studied numerically using Monte-Carlo methods in fractional Burgers flows subject to additive colored noise in [72]. The main finding was that there was no evidence for the noise to regularize the evolution by suppressing blow-up in the supercritical regime, or for the noise to trigger blow-up in the subcritical regime. However, as the noise amplitude becomes large, the blow-up times in the supercritical regime (understood as a random variable) were shown to exhibit an increasingly non-Gaussian behavior.

3. Estimates for the 2D Navier-Stokes System

Denoting $\omega(t, \mathbf{x}) := \omega(t, \mathbf{x}) \cdot \mathbf{e}_3$ the vorticity component perpendicular to the plane of motion, where \mathbf{e}_3 is the corresponding unit vector of the Cartesian coordinate system, the 2D Navier-Stokes system can be written as

$$\frac{\partial \omega}{\partial t} + J(\omega, \psi) = \nu \Delta \omega \quad \text{in } (0, T] \times \Omega, \quad (3.1a)$$

$$-\Delta \psi = \omega \quad \text{in } (0, T] \times \Omega, \quad (3.1b)$$

$$\omega(0) = \omega_0 \quad (3.1c)$$

where $\Omega = \mathbb{T}^2$ is a doubly-periodic domain, ψ the streamfunction, whereas $J(f, g) := \partial_x f \partial_y g - \partial_y f \partial_x g$ defined for some functions $f, g : \Omega \rightarrow \mathbb{R}$ is the Jacobian determinant. As is well known [3], system (3.1) is globally well posed in the classical sense.

In the absence of vortex stretching in (3.1a), the cubic term responsible for the production of enstrophy in (1.9b) vanishes identically, such that for 2D flows on domains without solid boundaries we have $d\mathcal{E}(\psi(t))/dt \leq 0, t \geq 0$ (for convenience, here we assume the streamfunction ψ to be the main state variable). Thus, in such cases the enstrophy is a nonincreasing function of time and hence is rather uninteresting.

On the other hand, by computing the gradient of equation (3.1a) we obtain the equation describing the evolution of the vorticity gradient $\nabla \omega$

$$\frac{\partial \nabla \omega}{\partial t} + (\mathbf{u} \cdot \nabla) \nabla \omega = \nu \Delta \nabla \omega - [\nabla \mathbf{u}]^T \cdot \nabla \omega, \quad (3.2)$$

where the velocity field is given by $\mathbf{u} = \nabla^\perp \psi$ with $\nabla^\perp := [\partial/\partial y, -\partial/\partial x]$ and the palinstrophy

$$\mathcal{P}(\psi(t)) := \frac{1}{2} \int_{\Omega} |\nabla \Delta \psi(t, \mathbf{x})|^2 d\Omega \quad (3.3)$$

plays the role of “energy”. Since equation (3.2) features a quadratic stretching term $[\nabla \mathbf{u}]^T \cdot \nabla \omega$, palinstrophy may exhibit nontrivial growth in 2D Navier-Stokes flows, as opposed to energy and enstrophy. Hence, it serves as a key measure of extreme behavior possible in such flows and its rate of growth describing the build-up of vorticity gradients can be obtained from (3.2) as

$$\frac{d\mathcal{P}(\psi(t))}{dt} = \int_{\Omega} J(\Delta \psi, \psi) \Delta^2 \psi d\Omega - \nu \int_{\Omega} (\Delta^2 \psi)^2 d\Omega =: \mathcal{R}_{\mathcal{P}}(\psi). \quad (3.4)$$

In analogy with the results discussed in Section 2, the goal of this study was to characterize the largest growth of palinstrophy possible instantaneously and in finite time. As a first step, the following estimate on the rate of growth of palinstrophy was obtained in [9]

$$\frac{d\mathcal{P}}{dt} \leq \frac{C}{\nu} \mathcal{K}^{\frac{1}{2}} \mathcal{P}^{\frac{3}{2}}. \quad (3.5)$$

We note that, in contrast to the estimates on the rate of growth of enstrophy in 1D and in 3D, cf. (1.10) and (2.3), the upper bound in (3.5) is a function of two quantities, i.e., the energy \mathcal{K} and palinstrophy \mathcal{P} . The former quantity could be eliminated from (3.5) in favor of \mathcal{P} using nested Poincaré’s inequalities $\mathcal{K} \leq (2\pi)^{-4} \mathcal{P}$ which would give $d\mathcal{P}/dt \leq (C/\nu) \mathcal{P}^2$, however, sharpness would be lost in this process. Estimate (3.5) was refined in [73] where a sharper form of the prefactor dependent on \mathcal{K} was obtained

$$\frac{d\mathcal{P}}{dt} \leq \left(a + b\sqrt{\ln Re + c} \right) \mathcal{P}^{\frac{3}{2}} \quad \text{with } a=0, b=\sqrt{2\pi}, c=-\ln\left(\frac{2}{\sqrt{\pi}}\right) \quad (3.6)$$

and with the Reynolds number defined as $Re := \mathcal{K}^{1/2}/\nu$. We add that, as was shown in [74] (see also [9]), some other estimates on $d\mathcal{P}/dt$ can be obtained, but they involve bounds on quantities such as $\|\Delta \omega\|_{L^2(\Omega)}$ and $\|\omega\|_{L^\infty(\Omega)}$ which are hard to control. Estimates on the rate of growth of palinstrophy in the presence of external body forces were obtained in [75].

By integrating the instantaneous estimate (3.6) with respect to time, the following finite-time bound was obtained in [73]

$$\max_{t \geq 0} \mathcal{P}(\psi(t)) \leq \Phi(Re_0) \mathcal{P}_0 \quad \text{with} \quad \Phi(Re_0) := \left(1 + \frac{a + b\sqrt{\ln Re_0 + c}}{4} Re_0\right)^2, \quad (3.7)$$

where $Re_0 := \mathcal{K}_0^{1/2}/\nu$ and $\mathcal{P}_0 := \mathcal{P}(\psi(0))$. In order to assess sharpness of instantaneous estimates (3.5)–(3.6) with respect to \mathcal{K} and \mathcal{P} , the following optimization problem was formulated in [9]

Problem 3. Given $\mathcal{K}_0, \mathcal{P}_0 \in \mathbb{R}_+$ and the objective functional $\mathcal{R}_{\mathcal{P}_0}(\psi)$, cf. (3.4), find

$$\begin{aligned} \tilde{\psi}_{\mathcal{K}_0, \mathcal{P}_0} &= \arg \max_{\psi \in \mathcal{W}_{\mathcal{K}_0, \mathcal{P}_0}} \mathcal{R}_{\mathcal{P}_0}(\psi), \quad \text{where} \\ \mathcal{W}_{\mathcal{K}_0, \mathcal{P}_0} &= \left\{ \psi \in H^4(\Omega) : \frac{1}{2} \int_{\Omega} |\nabla \psi|^2 d\Omega = \mathcal{K}_0, \frac{1}{2} \int_{\Omega} |\nabla \Delta \psi|^2 d\Omega = \mathcal{P}_0 \right\}. \end{aligned}$$

We emphasize that in contrast to Problem 1, Problem 3 involves two constraints which is motivated by the structure of the upper bounds in estimates (3.5)–(3.6) and makes it harder to solve numerically, cf. comments at the end of Appendix (a). Local maximizers of Problem 3 with $\nu = 10^{-3}$ were found in [9] for a broad range of values of \mathcal{K}_0 and \mathcal{P}_0 , where we focused on the dependence of $\mathcal{R}_{\mathcal{P}_0}(\tilde{\psi}_{\mathcal{K}_0, \mathcal{P}_0})$ on \mathcal{P}_0 with the kinetic energy \mathcal{K}_0 held fixed. A representative maximizer $\tilde{\psi}_{\mathcal{K}_0, \mathcal{P}_0}$ is shown in terms of the corresponding vorticity field $-\Delta \tilde{\psi}_{\mathcal{K}_0, \mathcal{P}_0}$ in Figure 2a. As is evident from this figure, the optimal state involves a quadrupole vortex generating a straining field that stretches a vortex filament located at the center. As demonstrated in [73], for fixed \mathcal{K}_0 the optimizers $\tilde{\psi}_{\mathcal{K}_0, \mathcal{P}_0}$ are self-similar with respect to \mathcal{P}_0 , i.e., they admit the representation $\tilde{\psi}_{\mathcal{K}_0, \mathcal{P}_0} = \mathcal{P}_0^\beta \Psi(\mathcal{P}_0^q \mathbf{x})$, where the rational exponents β and q are determined from the constraints and the optimality conditions in Problem 3, whereas Ψ is a function independent of \mathcal{P}_0 , but depending on \mathcal{K}_0 . We also note that in the small-palinstrophy limit defined by Poincaré's inequality $\mathcal{P}_0 \rightarrow (2\pi)^4 \mathcal{K}_0$, the cubic term in (3.4) vanishes which simplifies Problem 3 since the objective function becomes quadratic. This limiting problem can be solved in closed form using the method of Lagrange multipliers with the maximizers $\tilde{\psi}_{\mathcal{K}_0, \mathcal{P}_0}$ having the form of eigenfunctions of the Laplacian.

In [9] we were interested in sharpness of the instantaneous estimate (3.5) with respect to \mathcal{P}_0 and this is verified in Figure 2b where we plot $\mathcal{R}_{\mathcal{P}_0}(\tilde{\psi}_{\mathcal{K}_0, \mathcal{P}_0})$ as function of \mathcal{P}_0 for different values of \mathcal{K}_0 , revealing a power-law dependence of the form $\mathcal{R}_{\mathcal{P}_0}(\tilde{\psi}_{\mathcal{K}_0, \mathcal{P}_0}) \sim \mathcal{O}(\mathcal{P}_0^{3/2})$ for large \mathcal{P}_0 . Sharpness of the refined estimate (3.6) with respect to the second parameter \mathcal{K}_0 was then established in [73] by analyzing solutions of Problem 3, although the parameters a, b and c were found to have values different from the values given in (3.6).

As regards the companion question about sharpness of the finite-time estimate (3.7), in [73] it was shown that flow evolutions corresponding to the optimal initial data $\tilde{\psi}_{\mathcal{K}_0, \mathcal{P}_0}$ obtained by solving Problem 3 for fixed \mathcal{K}_0 and different \mathcal{P}_0 saturate the bound in estimate (3.7) with respect to \mathcal{P}_0 , in the sense that the maximum attained values of the palinstrophy $\max_{t \geq 0} \mathcal{P}(\psi(t))$ grow in proportion to \mathcal{P}_0 when \mathcal{K}_0 remains fixed. On the other hand, dependence of the prefactor $\Phi(Re_0)$ on Re_0 , or on \mathcal{K}_0 , was found to be more nuanced, which can be attributed to the fact that the flow trajectories considered correspond to initial data which is optimal in the instantaneous sense only. The vortex-dynamics mechanisms realizing the extreme flow behavior discussed above were analyzed in [10]. As is evident from Movie 1, the stretching of three thin parallel vortex filaments is the key effect responsible for the build-up of the palinstrophy. We add that since $d\mathcal{E}/dt = -\nu\mathcal{P}$ the question about the maximum growth of palinstrophy is related to the problem of the enstrophy dissipation vanishing in the limit $\nu \rightarrow 0$ in 2D turbulence [74,76].

Finally, we add that on bounded domains there are additional terms in expression (1.9b) for the rate of growth of enstrophy in the form of integrals over the domain boundary $\partial\Omega$, such that in 2D Navier-Stokes flows on such domains the enstrophy can grow. While we are unaware of any a priori estimates on $d\mathcal{E}/dt$ on bounded domains in 2D, the extreme behavior of this quantity

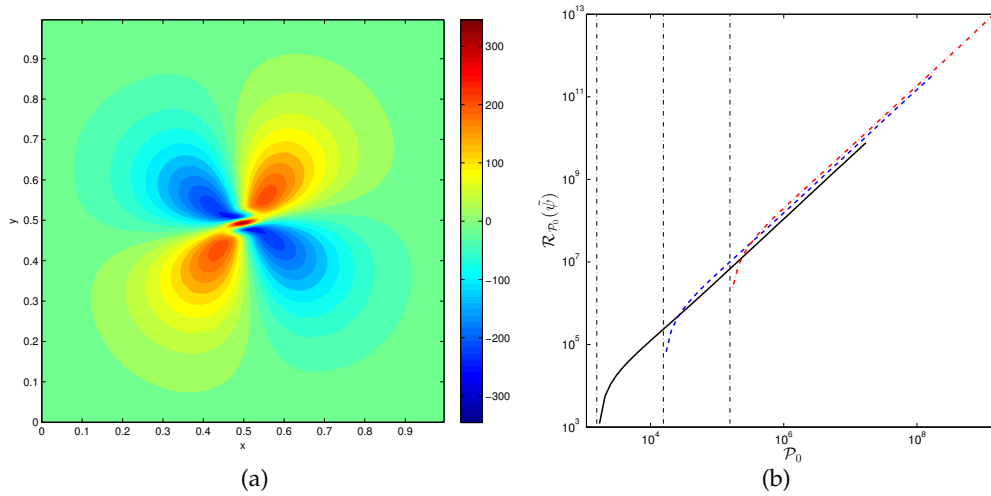


Figure 2. (a) Vorticity field $-\Delta\tilde{\psi}_{\mathcal{K}_0, \mathcal{P}_0}$ solving Problem 3 with $\mathcal{K}_0 = 10$ and $\mathcal{P}_0 = 1.5585 \cdot 10^6$. (b) Dependence of the maximum palinstrophy rate of growth $\mathcal{R}_{\mathcal{P}_0}(\tilde{\psi}_{\mathcal{K}_0, \mathcal{P}_0})$ on \mathcal{P}_0 for $\mathcal{K}_0 = 10^0, 10^1$ and 10^2 with the vertical lines representing the corresponding Poincaré limits $(2\pi)^4 \mathcal{K}_0$.

can be studied by solving suitable optimization problems and some preliminary results in this direction were reported in [77].

4. Estimates for the 3D Navier-Stokes System

The question about sharpness of the instantaneous estimate (1.10) was considered by Lu & Doering in [28] who formulated and studied the following optimization problem

Problem 4. Given $\mathcal{E}_0 \in \mathbb{R}_+$ and the objective functional $\mathcal{R}_{\mathcal{E}}(\mathbf{u})$, cf. (1.9b), find

$$\tilde{\mathbf{u}}_{\mathcal{E}_0} = \arg \max_{\mathbf{u} \in \mathcal{S}_{\mathcal{E}_0}} \mathcal{R}_{\mathcal{E}}(\mathbf{u}), \quad \text{where} \quad \mathcal{S}_{\mathcal{E}_0} := \left\{ \mathbf{u} \in H^2(\Omega) : \nabla \cdot \mathbf{u} = 0, \int_{\Omega} \mathbf{u} \, dx = \mathbf{0}, \mathcal{E}(\mathbf{u}) = \mathcal{E}_0 \right\}.$$

We remark that the numerical approach adopted in [28] was somewhat different from the methodology described in Appendix A in that it relied on a “discretize-then-optimize” formulation wherein Problem 4 was first discretized with a Fourier-Galerkin method which then lead to an optimization problem in a finite dimension. Using this approach over a range of values of \mathcal{E}_0 and with $\nu = 10^{-2}$, Lu & Doering found two branches of locally maximizing solutions $\tilde{\mathbf{u}}_{\mathcal{E}_0}$ of Problem 4, with one branch characterized by the relation³

$$\mathcal{R}(\tilde{\mathbf{u}}_{\mathcal{E}_0}) \sim 3.59 \cdot 10^{-3} \mathcal{E}_0^{2.997} \quad \text{as} \quad \mathcal{E}_0 \rightarrow \infty. \quad (4.1)$$

Thus, the maximizers on this branch, which interestingly have the form of two colliding nearly axisymmetric vortex rings, saturate estimate (1.10) in the sense that the rate at which these maximizers produce enstrophy increases in proportion to \mathcal{E}_0^3 (although the numerical prefactor in (4.1) is smaller than the one in estimate (1.10) by about 9 orders of magnitude). These maximizers are strongly localized such that as the enstrophy increases the characteristic radius of the vortex rings vanishes as $\mathcal{O}(\mathcal{E}_0^{-1})$ [11]. The maximizers associated with the second branch were characterized by the asymptotic relation $\mathcal{R}(\tilde{\mathbf{u}}_{\mathcal{E}_0}) \sim 0.299 \mathcal{E}_0^{1.78}$ and involved vorticity concentrated in four rod-like regions.

³Due to the presence of the factor 1/2 in (1.3b), the coefficient in (4.1) differs from that given in [28].

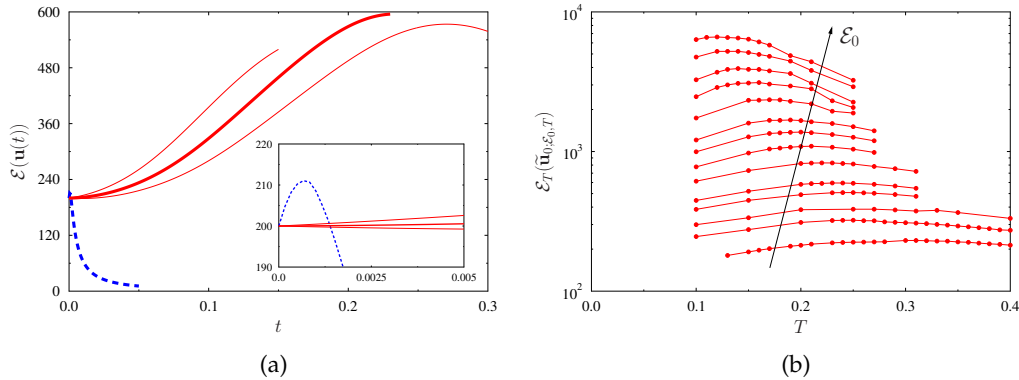


Figure 3. (a) Enstrophy $\mathcal{E}(\mathbf{u}(t))$ as a function of time t obtained from the solution of the Navier-Stokes system (1.1) with the initial condition \mathbf{u}_0 given by (blue dashed line) the maximizer $\tilde{\mathbf{u}}_{\mathcal{E}_0}$ of Problem 4 and (red solid lines) the asymmetric maximizers $\tilde{\mathbf{u}}_{0,\mathcal{E}_0,T}$ of Problem 5 for $\mathcal{E}_0 = 200$ and $T = 0.15, 0.23, 0.3$ (the curve corresponding to the optimal length of the time window $\tilde{T}_{\mathcal{E}_0} = 0.23$ is marked with a thick line whereas the inset represents magnification of the initial stages of evolution). (b) Maximum attained enstrophy $\mathcal{E}_T(\tilde{\mathbf{u}}_{0,\mathcal{E}_0,T})$ as a function of the length T of the window over which maximization is performed in Problem 5 for initial entropies $100 \leq \mathcal{E}_0 \leq 1000$ (the trend with the increase of \mathcal{E}_0 is indicated with an arrow). Each curve corresponds to flow evolutions starting from asymmetric optimal initial conditions $\tilde{\mathbf{u}}_{0,\mathcal{E}_0,T}$ with the same value of the initial enstrophy and different T (solid symbols represent the values of \mathcal{E}_0 and T for which local maximizers of Problem 5 were found).

Problem 4 was revisited in [11] where we recomputed the asymptotically dominating branch with more accuracy which allowed us to slightly improve the prefactor in (4.1) to $3.72 \cdot 10^{-3}$. We also considered the problem in the limit $\mathcal{E}_0 \rightarrow 0$ in which it was shown to admit closed-form solutions $\tilde{\mathbf{u}}_{\mathcal{E}_0}$ in the form of divergence-free eigenfunctions of the vector Laplacian. One of these limiting maximizers is the Taylor-Green vortex, which has been employed as the initial data in a number of studies aimed at triggering singular behaviour in both the Euler and Navier-Stokes systems [32,34,43,78]. It is interesting that the Taylor-Green vortex arises as a solution of Problem 4 in the limit $\mathcal{E}_0 \rightarrow 0$.

The time evolution of solutions of the Navier-Stokes system (1.1) with the maximizers $\tilde{\mathbf{u}}_{\mathcal{E}_0}$ of Problem 4 used as initial data was considered in [11]. It was shown that while at $t=0$ the enstrophy in these flows is generated at the maximum rate given in (4.1), this rate is very quickly depleted such that in finite time only little enstrophy is produced, cf Figure 3a. The flow evolution remains essentially axisymmetric with the vortex rings approaching each other before starting to diffuse. The key conclusion from these results is that if a significant, let alone unbounded, growth of enstrophy is to be achieved in finite time, it must be associated with initial data \mathbf{u}_0 other than the extreme vortex states $\tilde{\mathbf{u}}_{\mathcal{E}_0}$ saturating the upper bound in estimate (1.10) on the instantaneous rate of growth of enstrophy, cf. (4.1).

More specifically, assuming the instantaneous rate of growth of enstrophy in the form $d\mathcal{E}/dt = C \mathcal{E}^\alpha$ with some prefactor $C > 0$, any exponent $\alpha > 2$ will cause $\mathcal{E}(\mathbf{u}(t))$ to become unbounded at some finite time $t_0 = t_0(\alpha)$ if this rate of growth is sustained over the interval $[0, t_0)$. The fact that there is no blow-up when $1 < \alpha \leq 2$ follows from the observation that one factor of \mathcal{E} in (1.10) can be bounded in terms of the initial energy \mathcal{K}_0 using (1.9a) as follows

$$\int_0^t \mathcal{E}(\mathbf{u}(s)) ds = \frac{1}{2\nu} [\mathcal{K}_0 - \mathcal{K}(\mathbf{u}(t))] \leq \frac{1}{2\nu} \mathcal{K}_0, \quad (4.2)$$

which upon applying Grönwall's lemma to $d\mathcal{E}/dt = C \mathcal{E}^\alpha$ with $\alpha = 2$ yields the bound

$$\max_{0 \leq t \leq T} \mathcal{E}(\mathbf{u}(t)) \leq \mathcal{E}_0 \exp \left[C \int_0^T \mathcal{E}(\mathbf{u}(s)) ds \right] \leq \mathcal{E}_0 \exp \left[\frac{C}{2\nu} \mathcal{K}_0 \right]. \quad (4.3)$$

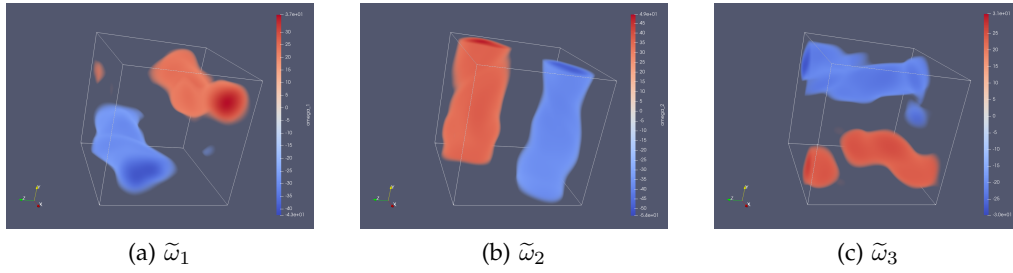


Figure 4. Vorticity components of the asymmetric optimal initial condition $\tilde{\mathbf{u}}_{0;\mathcal{E}_0,\tilde{T}_{\mathcal{E}_0}}$ obtained by solving Problem 5 for the initial enstrophy $\mathcal{E}_0 = 500$ and the corresponding optimal length $\tilde{T}_{\mathcal{E}_0} = 0.17$ of the time interval. The time evolution of the flow corresponding to this initial condition is visualized in Movie 2.

Evidently, as the rate of growth of enstrophy slows down when $\alpha \rightarrow 2^+$, for blow-up to occur this minimum growth rate must be sustained over windows of time with increasing length, i.e., $t_0 \rightarrow \infty$ as $\alpha \rightarrow 2^+$. To assess the feasibility of such a scenario, the following optimization problem was considered in [13]

Problem 5. Given $\mathcal{E}_0, T \in \mathbb{R}_+$ and the objective functional $\mathcal{E}_T(\mathbf{u}_0) := \mathcal{E}(\mathbf{u}(T))$, find

$$\tilde{\mathbf{u}}_{0;\mathcal{E}_0,T} = \arg \max_{\mathbf{u}_0 \in \mathcal{Q}_{\mathcal{E}_0}} \mathcal{E}_T(\mathbf{u}_0), \quad \text{where } \mathcal{Q}_{\mathcal{E}_0} := \left\{ \mathbf{u}_0 \in H^1(\Omega) : \nabla \cdot \mathbf{u}_0 = 0, \int_{\Omega} \mathbf{u}_0 \, d\mathbf{x} = \mathbf{0}, \mathcal{E}(\mathbf{u}_0) = \mathcal{E}_0 \right\}.$$

While Problem 5 is quite challenging from the computational point of view, optimal solutions $\tilde{\mathbf{u}}_{0;\mathcal{E}_0,T}$ were found in [13] for a range of values of \mathcal{E}_0 and T with $\nu = 10^{-2}$. They belong to two distinct branches, referred to as “symmetric” and “asymmetric”, with the extreme flows corresponding to the initial data $\tilde{\mathbf{u}}_{0;\mathcal{E}_0,T}$ on the symmetric branch exhibiting equipartition of enstrophy among the three Cartesian coordinate dimensions. For large values of the initial enstrophy \mathcal{E}_0 the asymmetric branch dominates in the sense that the corresponding Navier-Stokes flows achieve higher values of $\mathcal{E}_T(\tilde{\mathbf{u}}_{0;\mathcal{E}_0,T})$ than the flows with initial data on the symmetric branch for the same values of \mathcal{E}_0 and T . The time evolution of the enstrophy $\mathcal{E}(\mathbf{u}(t))$ in the extreme flows with the asymmetric initial conditions $\tilde{\mathbf{u}}_{0;\mathcal{E}_0,T}$ obtained for a fixed $\mathcal{E}_0 = 200$ and different time windows T is shown in Figure 3a, where we see that in these flows a much larger growth of enstrophy is achieved than in the flow with the instantaneously optimal initial condition $\tilde{\mathbf{u}}_{\mathcal{E}_0}$ obtained by solving Problem 4 for the same value of \mathcal{E}_0 . Interestingly, we notice that for some values of T the enstrophy $\mathcal{E}(\mathbf{u}(t))$ is in fact decreasing at early times before it starts to grow. A typical asymmetric initial condition $\tilde{\mathbf{u}}_{0;\mathcal{E}_0,T}$ is shown in Figure 4 where it is evident that it has the form of three perpendicular pairs of antiparallel vortex tubes. The evolution of the flow corresponding to this initial condition is visualized in Movie 2. Interestingly, all extreme flows with initial conditions found by solving Problem 5 have zero helicity $\mathcal{H}(\mathbf{u}(t)) := \int_{\Omega} \mathbf{u}(t) \cdot (\nabla \times \mathbf{u}(t)) \, d\mathbf{x} = 0, t \geq 0$.

No evidence has been found for unbounded growth of enstrophy that would signal singularity formation, cf. condition (1.4), in Navier-Stokes flows with initial data obtained as solutions of Problem 5 for a broad range of values of \mathcal{E}_0 and T . The maximum enstrophy values $\mathcal{E}_T(\tilde{\mathbf{u}}_{0;\mathcal{E}_0,T})$ attained with asymmetric initial conditions $\tilde{\mathbf{u}}_{0;\mathcal{E}_0,T}$ are shown as functions of the optimization window T for different values of \mathcal{E}_0 in Figure 3b. We see that the branches of maximizers corresponding to different values of \mathcal{E}_0 all exhibit well-defined unique maxima attained at times $\tilde{T}_{\mathcal{E}_0} = \arg \max_{T > 0} \mathcal{E}_T(\tilde{\mathbf{u}}_{0;\mathcal{E}_0,T}), \forall \mathcal{E}_0$, which decrease as $\mathcal{O}(\mathcal{E}_0^{-1/2})$. These maximum enstrophy values $\mathcal{E}_{\tilde{T}_{\mathcal{E}_0}}(\tilde{\mathbf{u}}_{0;\mathcal{E}_0,\tilde{T}_{\mathcal{E}_0}})$ are plotted as a function of \mathcal{E}_0 in Figure 5a revealing a power-law relation

$$\max_{T > 0} \mathcal{E}_T(\tilde{\mathbf{u}}_{0;\mathcal{E}_0,T}) \sim (0.224 \pm 0.006) \mathcal{E}_0^{1.490 \pm 0.004}. \quad (4.4)$$

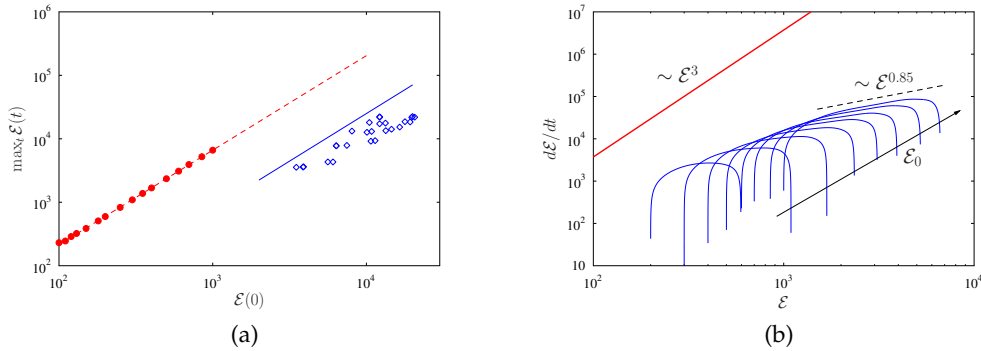


Figure 5. (a) Dependence of the maximum attained enstrophy $\max_{t \geq 0} \mathcal{E}(t)$ on the initial enstrophy $\mathcal{E}(0)$ in Navier-Stokes flows with the optimal initial conditions (red solid circles) $\tilde{\mathbf{u}}_{0;\mathcal{E}_0,T}$ obtained by solving Problems 5 (the asymmetric branch) and (blue diamonds) $\tilde{\mathbf{u}}_{0;B,T}$ obtained by solving Problem 6 (the partially-symmetric branch). For the local maximizers of Problems 5 each symbol corresponds to a different value of the constraint \mathcal{E}_0 , and in all cases the results are presented for the optimization window with length T producing the largest value of $\max_{t \geq 0} \mathcal{E}(t)$. For Problem 6 the symbols correspond to local maximizers obtained with different values of B and T , whereas the straight lines represent the relation $\max_{t \geq 0} \mathcal{E}(t) \approx C\mathcal{E}_0^{3/2}$ with different prefactors C . (b) Flow trajectories corresponding to the optimal initial data $\tilde{\mathbf{u}}_{0;\mathcal{E}_0,\tilde{T}_{\mathcal{E}_0}}$ obtained by solving Problem 5 with different $\mathcal{E}_0 \in [100, 1000]$ shown using the coordinates $\{\mathcal{E}, d\mathcal{E}/dt\}$ (blue solid lines with the arrow indicating the trend with the increase of \mathcal{E}_0). The thick red line represents the relation $d\mathcal{E}/dt = 3.72 \cdot 10^{-3} \mathcal{E}^3$ found in [11], whereas the dashed black line the relation $d\mathcal{E}/dt = 10^2 \mathcal{E}^{0.85}$.

In order to understand how close the flow evolutions corresponding to the optimal initial data $\tilde{\mathbf{u}}_{0;\mathcal{E}_0,\tilde{T}_{\mathcal{E}_0}}$ come to saturating a priori bounds on the rate of growth of enstrophy, cf. (1.10), in Figure 5b we plot the corresponding trajectories using the coordinates $\{\mathcal{E}, d\mathcal{E}/dt\}$, such that each trajectory is parameterized by time t (since the logarithmic scale is used, initial parts of the trajectories when $d\mathcal{E}/dt \lesssim 0$ are not shown). The slope of the tangent to each of the curves thus represents the exponent α characterizing the instantaneous rate of enstrophy production $d\mathcal{E}/dt \sim \mathcal{E}^\alpha$. In Figure 5b we also indicate the relation $d\mathcal{E}/dt = 3.72 \cdot 10^{-3} \mathcal{E}^3$ describing the maximum rate of enstrophy growth realized by solutions of Problem 4 [11,28]. We observe that the rate of growth of enstrophy achieved along the trajectories corresponding to the optimal initial conditions $\tilde{\mathbf{u}}_{0;\mathcal{E}_0,\tilde{T}_{\mathcal{E}_0}}$ is at all times and for all values of \mathcal{E}_0 several orders of magnitude smaller than the maximum rate of growth achieved by the instantaneous maximizers $\tilde{\mathbf{u}}_{\mathcal{E}_0}$. We also note that at the final stages of the flow evolutions before the enstrophy maximum is reached at $t = \tilde{T}_{\mathcal{E}_0}$ the enstrophy is amplified at an approximate rate $d\mathcal{E}/dt \sim \mathcal{E}^{0.85}$, far below the minimum rate of growth $d\mathcal{E}/dt \sim \mathcal{E}^\alpha$ with $2 < \alpha \leq 3$ needed for enstrophy to become unbounded in finite time.

In a recent study [24] we have considered the Ladyzhenskaya-Prodi-Serrin condition (1.7) focusing on the case with $q = 4$ and $p = 8$, which is the pair of integer-valued indices closest to the critical case with $q = 3$, cf. (1.6). The goal was to search for potential finite-time singularities in Navier-Stokes flows governed by (1.1) by maximizing the quantity

$$\Phi_T(\mathbf{u}_0) := \frac{1}{T} \int_0^T \|\mathbf{u}(\tau)\|_{L^4(\Omega)}^8 d\tau \quad (4.5)$$

with respect to the initial condition \mathbf{u}_0 where a natural function space for the initial data would be $L^4(\Omega)$ and the constraint would have the form $\|\mathbf{u}_0\|_{L^4} = B$ for some $0 \leq B \leq \infty$. However, from the computational point of view, PDE-constrained optimization problems are formulated most conveniently in a Hilbert space [79]. While there exist solution approaches applicable in the more general setting of Banach spaces, e.g., [80], they are significantly harder to use in practice. Given the form of the constraint, we have chosen to formulate the optimization problem in the “largest” Sobolev space with Hilbert structure contained in $L^4(\Omega)$. From the Sobolev embedding theorem

in dimension 3 [14], we deduce

$$H^s(\Omega) \hookrightarrow L^4(\Omega), \quad s \geq \frac{3}{4}, \quad (4.6)$$

such that the largest Hilbert-Sobolev space embedded in $L^4(\Omega)$ is the space $H^{3/4}(\Omega)$. Thus, this leads to the following optimization problem

Problem 6. Given $B, T \in \mathbb{R}_+$ and the objective functional $\Phi_T(\mathbf{u}_0)$ from equation (4.5), find

$$\begin{aligned} \tilde{\mathbf{u}}_{0;B,T} &= \arg \max_{\mathbf{u}_0 \in \mathcal{L}_B} \Phi_T(\mathbf{u}_0), \quad \text{where} \\ \mathcal{L}_B &:= \left\{ \mathbf{u}_0 \in H^{3/4}(\Omega) : \nabla \cdot \mathbf{u}_0 = 0, \int_{\Omega} \mathbf{u}_0 \, d\mathbf{x} = \mathbf{0}, \|\mathbf{u}_0\|_{L^4(\Omega)} = B \right\}. \end{aligned}$$

Local maximizers of Problem 6 were found in [24] for a range of values of B and T using a numerical procedure which is an extension of the approach described in Appendix A, where the main modification concerned the handling of the non-quadratic constraint in the definition of the manifold \mathcal{L}_B . Two branches of maximizers were discovered with partially symmetric and asymmetric optimal initial conditions $\tilde{\mathbf{u}}_{0;B,T}$. In this case as well no evidence was found for unbounded growth of the quantity $\Phi_T(\tilde{\mathbf{u}}_{0;B,T})$ which would signal singularity formation. The maximum enstrophy attained in the extreme flows with the optimal initial conditions $\tilde{\mathbf{u}}_{0;B,T}$ on the partially symmetric branch obtained for different B and T is plotted as function of the initial enstrophy \mathcal{E}_0 in Figure 5a. It is intriguing to observe that the envelope of these data points, obtained by maximizing the largest attained enstrophy over B and T , is also described by the relation $\max_{t>0} \mathcal{E}(t) \sim C \mathcal{E}_0^{3/2}$, i.e., the same as found for flows corresponding to solutions of Problem 5, except that the prefactor C is smaller than in (4.4). Finally, by maximizing the quantity $\Psi_T(\mathbf{u}_0) := \frac{1}{T} \int_0^T \|\mathbf{u}(\tau)\|_{L^4(\Omega)}^{8/3} \, d\tau$ with respect to the initial data $\mathbf{u}_0 \in H^{3/4}(\Omega)$ and subject to the constraint $(1/2)\|\mathbf{u}_0\|_{L^2}^2 = \mathcal{K}_0$ for a range of $\mathcal{K}_0 > 0$ in an optimization problem analogous to Problem 6 we arrived at a conjecture that a priori estimate (1.8) may not sharp and can possibly be improved by reducing the exponent of \mathcal{K}_0 in the bound on the RHS. The validity of this conjecture depends on whether the local maximizers of $\Psi_T(\mathbf{u}_0)$ we found are also global maximizers.

5. Relation to Bounding Approaches

In this section we briefly discuss connections between the approaches and results surveyed above and other techniques for quantifying the extreme behavior possible in fluid flows. For brevity, we will assume here the solution $\mathbf{u}(t) \in \mathcal{X}$, where \mathcal{X} is a suitable Hilbert space of solutions (finite or infinite dimensional), satisfies the autonomous system $d\mathbf{u}(t)/dt = \mathbf{f}(\mathbf{u}(t))$ with some $\mathbf{f} : \mathcal{X} \rightarrow \mathcal{X}$ and the initial condition $\mathbf{u}(0) = \mathbf{u}_0 \in X \subset \mathcal{X}$, where the set X encodes the constraints imposed on \mathbf{u}_0 . Denoting $\varphi : \mathcal{X} \rightarrow \mathbb{R}$ the quantity of interest in Problems 2, 5 and 6, these problems can be expressed as

$$\bar{\varphi} := \sup_{\mathbf{u}_0 \in X} \varphi(\mathbf{u}(\cdot; \mathbf{u}_0)), \quad (5.1)$$

where $\mathbf{u}(t; \mathbf{u}_0)$ is the solution of the governing system at time t corresponding to the initial condition \mathbf{u}_0 . Since Problems 2, 5 and 6 are nonconvex, their solutions discussed in Sections 2 and 4 were obtained by *locally* maximizing φ over flow trajectories parameterized by the initial data \mathbf{u}_0 and hence may not saturate the global maxima $\bar{\varphi}$.

On the other hand, it is possible to obtain upper bounds on the supremum $\bar{\varphi}$ by exploiting the structure of the governing equation, yet without reference to individual trajectories. It has been shown in [66] that defining an auxiliary function $V : \mathcal{X} \rightarrow \mathbb{R}$ with the Lie derivative $\mathcal{L}V(\mathbf{u}(t)) := \langle \nabla V(\mathbf{u}(t)), \mathbf{f}(\mathbf{u}(t)) \rangle_{\mathcal{X}} = dV(\mathbf{u}(t))/dt$, such upper bounds can be deduced by solving

the following optimization problem

$$\bar{\varphi} \leq \inf_V \sup_{\mathbf{u} \in X} V(\mathbf{u}), \quad (5.2a)$$

$$\mathcal{L}V(\mathbf{u}) \leq 0, \quad \mathbf{u} \in \mathcal{X}, \quad (5.2b)$$

$$\varphi(\mathbf{u}) - V(\mathbf{u}) \leq 0, \quad \mathbf{u} \in \mathcal{X}, \quad (5.2c)$$

which is independent of any particular solution trajectories. Importantly, in contrast to problem (5.1), the outer minimization problem in (5.2a) is convex and the two problems are dual to each other [81] (under some additional conditions this duality is strong). In certain simple cases problem (5.2) can be solved analytically. Its numerical solution is in principle possible provided the inner maximization subproblem in (5.2a) can be suitably relaxed and the set of auxiliary functions V is made finite-dimensional. For example, when the auxiliary function $V(\mathbf{u})$ and the function $\mathbf{f}(\mathbf{u})$ in the governing system are polynomial, inequality constraint (5.2b) can be interpreted as imposing the non-negativity of a polynomial which can then be expressed in terms of a sum of squares (SoS) of some polynomial basis functions. For PDE problems a polynomial representation of $\mathbf{f}(\mathbf{u})$ can be constructed using a truncated Galerkin projection. These steps make it possible to approximate problem (5.2) in terms of a semi-definite optimization program for which many robust solution algorithms and software packages are available.

The auxiliary function $V(\mathbf{u})$ used in (5.2) is related to the Lyapunov function employed in the study of nonlinear stability of fixed points (except that, unlike the Lyapunov function, it need not be positive semi-definite). Formulations based on auxiliary functions can also be used to obtain bounds on infinite-time and space averages of various quantities of interest leading to convex optimization problems analogous to (5.2) [82–86]. When the auxiliary function is fixed and quadratic whereas optimization is performed with respect to the form of a certain “background flow”, this bounding framework reduces to the background method originally developed by Doering & Constantin [87] to obtain rigorous a priori bounds on energy dissipation in wall-bounded flows. The background method has been since used, both analytically and computationally, to derive bounds on average quantities in different flows and we refer the reader to [88] for a recent survey of this topic.

In relation to the results reviewed in Sections 2 and 3, in [66] the authors used a formulation based on auxiliary functions to rederive the a priori bounds (2.4) and (3.7), and to generalize the former for the case of the “fractional” enstrophy $\mathcal{E}_\alpha(u(t)) := \frac{1}{2} \int_0^1 |-\Delta^{\alpha/2} u(t, x)|^2 dx$ relevant when the evolution is governed by the fractional Burgers system (2.8). In addition, by solving optimization problem (5.2) for a Galerkin truncation of the Burgers system (2.1) and a range of values of \mathcal{E}_0 they were able to obtain upper bounds on $\mathcal{E}_T(\mathbf{u}_0)$ consistent with relation (2.7). This is a remarkable example of a situation when the lower and upper bounds found by solving problems (5.1) and (5.2) coincide effectively closing the duality gap. Problems 5 and 6 can also be put in the framework of (5.2) and it is interesting to see whether it may be possible to develop suitable truncations and relaxations for the inner maximization problem what will yield computationally tractable semi-definite optimization programs.

6. Summary and Conclusions

In this paper we have presented a survey of recent progress in the research program focused on a systematic computational search for extreme behavior in different hydrodynamic models. Motivated by open questions concerning the possibility of a finite-time blow-up in solutions of the Navier-Stokes system (1.1) in 3D, these investigations relied on solution of PDE-constrained optimization problems with objective functionals chosen based on certain conditional regularity results and a priori estimates available for different models. Families of local maximizers of these PDE optimization problems were determined numerically using state-of-the-art adjoint-based gradient approaches formulated in the continuous (infinite-dimensional) setting, cf. Appendix A. We note that in addition to their numerous successful practical applications involving, for

Table 1. Summary of a priori estimates considered in the research program discussed here together with information about their realizability.

PROBLEM	ESTIMATE	REALIZABILITY
1D Burgers instantaneous	$\frac{d\mathcal{E}}{dt} \leq \frac{3}{2} \left(\frac{1}{\pi^2\nu}\right)^{1/3} \mathcal{E}^{5/3}$	YES [28]
1D Burgers finite-time	$\max_{t \in [0, T]} \mathcal{E}(u(t)) \leq \left[\mathcal{E}_0^{1/3} + \frac{1}{16} \left(\frac{1}{\pi^2\nu}\right)^{4/3} \mathcal{E}_0 \right]^3$	NO [8,64–66]
2D Navier-Stokes instantaneous	$\frac{d\mathcal{P}}{dt} \leq C_2 \sqrt{\log(\mathcal{K}^{1/2}/\nu)} \mathcal{P}^{3/2}$	YES [9,73]
2D Navier-Stokes finite-time	$\max_{t \geq 0} \mathcal{P}(\mathbf{u}(t)) \leq \left(1 + \frac{a+b\sqrt{\ln Re_0+c}}{4} Re_0\right)^2 \mathcal{P}_0$	YES [9,73]
3D Navier-Stokes instantaneous	$\frac{d\mathcal{E}}{dt} \leq \frac{27}{8\pi^4\nu^3} \mathcal{E}^3$	YES [11,28]
3D Navier-Stokes finite-time	$\mathcal{E}(\mathbf{u}(t)) \leq \frac{\mathcal{E}_0}{\sqrt{1 - 4\frac{C\mathcal{E}_0^2}{\nu^3}t}}$ $\int_0^T \ \mathbf{u}(\tau)\ _{L^4(\Omega)}^{8/3} d\tau \leq C \mathcal{K}_0^{4/3}$	NO (???) [13,24]

example, shape optimization in aerodynamics [89] and data assimilation in numerical weather prediction [90], similar optimization approaches have also been employed in the study of some other fundamental problems in fluid mechanics, namely, optimal mixing [91,92], transition to turbulence [93] and search for rare events in turbulence based on instantons [94].

The main results of the research program are summarized in Table 1. The main conclusion is that so far our search based on the enstrophy and the Ladyzhenskaya-Prodi-Serrin conditions (1.4) and (1.5) has revealed no indication of singularity formation in 3D Navier-Stokes flows with the optimal initial conditions. However, the behavior exhibited by these different extreme flows in terms of the maximum growth of enstrophy is in fact similar, cf. Figure 5a, and analogous to what was found in 1D Burgers flows, cf. (2.7), (4.4) and Figure 1b. The results discussed in Section 3 demonstrated the sharpness of a number of a priori estimates on the growth of palinstrophy in 2D, both instantaneously and in finite time. We remark that the power-law structure of estimates (1.10), (3.5) and of the empirical relation (4.4) can be justified with simple arguments based on dimensional analysis [13,28,73]. The results surveyed here were obtained using different values of the viscosity coefficient ν . To facilitate quantitative comparison between different problems, they can be rescaled to correspond to say $\nu = 1$ expressing the solution of (1.1) as $\mathbf{u}(t, \mathbf{x}) =: \nu \mathbf{v}(\nu t, \mathbf{x})$, such that the rescaled solution \mathbf{v} solves (1.1) with $\nu = 1$ and the time variable redefined as νt (analogous approach applies to systems (2.1) and (3.1)).

Somewhat paradoxically, the situation in 2D is more satisfactory than in 1D where the key finite-time estimate (2.4) appears not to be sharp, as indicated by the agreement of the results discussed in Section 2, cf. (2.7), and the upper bounds found in [66] by solving problem (5.2). Thus, rigorously improving this estimate remains an open problem in PDE analysis and important progress towards this goal has already been made in [64,65]. More specifically, it is interesting to see whether the asymptotic estimate $\mathcal{O}(\mathcal{E}_0^{3/2})$ obtained in [64] for the maximum growth of enstrophy implies a rigorous upper bound on $\max_{t \geq 0} \mathcal{E}(t)$ and whether the required assumptions on the regularity of the initial data can be weakened.

Moving forward, the search for singular behavior in 3D Navier-Stokes flows can be broadened by considering optimization problems analogous to Problem 6 with objective functionals based on conditional regularity results generalizing (1.5) to include norms of derivatives of different

order of the velocity field [20]. In addition, this research program will be broadened to include search for potential singularities in 3D Euler flows which can be sought with similar approaches.

A. Solution of Optimization Problems

In this appendix we provide some comments about the numerical approaches employed to find families of local maximizers in the optimization problems discussed in Sections 2, 3 and 4. Since Problems 1–6 were designed to test certain subtle properties of the underlying PDEs, we chose to formulate the solution approaches in the continuous (“optimize-then-discretize”) setting, where the optimality conditions, constraints and gradient expressions are derived based on the original PDEs before being discretized for the purpose of numerical evaluation, instead of the alternative “discretize-then-optimize” approach often used in applications [60]. In general, local maximizers in Problems 1–6 can be approximated using discrete gradient flows with gradient expressions and constraints specific to different problems. To fix attention, here we will describe in some detail the approaches to solving Problems 4 and 5, and then provide comment how to adapt them to solve Problems 3 and 6 (Problem 1 is solvable analytically, whereas Problem 2 is a simpler 1D version of Problem 5). Finally, we will also provide some details about numerical approximations.

(a) Solution of Problem 4

For a given value of \mathcal{E}_0 , a local maximizer $\tilde{\mathbf{u}}_{\mathcal{E}_0}$ of Problem 4 can be found as $\tilde{\mathbf{u}}_{\mathcal{E}_0} = \lim_{n \rightarrow \infty} \mathbf{u}_{\mathcal{E}_0}^{(n)}$ using the following iterative procedure representing a discretization of a gradient flow projected on $\mathcal{S}_{\mathcal{E}_0}$

$$\begin{aligned} \mathbf{u}_{\mathcal{E}_0}^{(n+1)} &= \mathbb{P}_{\mathcal{S}_{\mathcal{E}_0}} \left(\mathbf{u}_{\mathcal{E}_0}^{(n)} + \tau_n \nabla \mathcal{R} \left(\mathbf{u}_{\mathcal{E}_0}^{(n)} \right) \right), \\ \mathbf{u}_{\mathcal{E}_0}^{(1)} &= \mathbf{u}^0, \end{aligned} \quad (\text{A } 1)$$

where $\mathbf{u}_{\mathcal{E}_0}^{(n)}$ is an approximation of the maximizer obtained at the n -th iteration, \mathbf{u}^0 is the initial guess and τ_n is the length of the step in the direction of the gradient $\nabla \mathcal{R}(\mathbf{u}_{\mathcal{E}_0}^{(n)})$. Projection onto the constraint manifold $\mathcal{S}_{\mathcal{E}_0}$ is performed using the composite operator $\mathbb{P}_{\mathcal{S}_{\mathcal{E}_0}} : H^2(\Omega) \rightarrow \mathcal{S}_{\mathcal{E}_0}$ defined as

$$\mathbb{P}_{\mathcal{S}_{\mathcal{E}_0}}(\mathbf{u}) = \mathcal{P}_{\mathcal{E}_0}(\Pi_0(\mathbf{u})), \quad \text{where} \quad (\text{A } 2a)$$

$$\Pi_0(\mathbf{u}) = \mathbf{u} - \nabla \left[\Delta^{-1}(\nabla \cdot \mathbf{u}) \right], \quad (\text{A } 2b)$$

$$\mathcal{P}_{\mathcal{E}_0}(\mathbf{u}) = \sqrt{\frac{\mathcal{E}_0}{\mathcal{E}(\mathbf{u})}} \mathbf{u} \quad (\text{A } 2c)$$

in which (A 2b) and (A 2c) represent, respectively, enforcement of the incompressibility condition and normalization related to the enstrophy constraint.

A key step in procedure (A 1) is evaluation of the gradient $\nabla \mathcal{R}(\mathbf{u})$ of the objective functional $\mathcal{R}(\mathbf{u})$, cf. (1.9b), representing its (infinite-dimensional) sensitivity to perturbations of the velocity field \mathbf{u} , and it is essential that the gradient be characterized by the required regularity, namely, $\nabla \mathcal{R}(\mathbf{u}) \in H^2(\Omega)$. This is, in fact, guaranteed by the Riesz representation theorem [81] applicable because the Gâteaux differential $\mathcal{R}'(\mathbf{u}; \cdot) : H^2(\Omega) \rightarrow \mathbb{R}$, defined as $\mathcal{R}'(\mathbf{u}; \mathbf{u}') := \lim_{\epsilon \rightarrow 0} \epsilon^{-1} [\mathcal{R}(\mathbf{u} + \epsilon \mathbf{u}') - \mathcal{R}(\mathbf{u})]$ for some perturbation $\mathbf{u}' \in H^2(\Omega)$, is a bounded linear functional on $H^2(\Omega)$. The Gâteaux differential can be computed directly to give

$$\mathcal{R}'(\mathbf{u}; \mathbf{u}') = \int_{\Omega} [\mathbf{u}' \cdot \nabla \mathbf{u} \cdot \Delta \mathbf{u} + \mathbf{u} \cdot \nabla \mathbf{u}' \cdot \Delta \mathbf{u} + \mathbf{u} \cdot \nabla \mathbf{u} \cdot \Delta \mathbf{u}'] dx - 2\nu \int_{\Omega} \Delta^2 \mathbf{u} \cdot \mathbf{u}' dx \quad (\text{A } 3)$$

from which, by the Riesz representation theorem, we obtain

$$\mathcal{R}'(\mathbf{u}; \mathbf{u}') = \left\langle \nabla \mathcal{R}(\mathbf{u}), \mathbf{u}' \right\rangle_{H^2(\Omega)} = \left\langle \nabla^{L^2} \mathcal{R}(\mathbf{u}), \mathbf{u}' \right\rangle_{L^2(\Omega)} \quad (\text{A } 4)$$

with the Riesz representers $\nabla\mathcal{R}(\mathbf{u})$ and $\nabla^{L^2}\mathcal{R}(\mathbf{u})$ being the gradients computed with respect to the H^2 and L^2 topology, respectively. We remark that, while the H^2 gradient is used exclusively in the actual computations, cf. (A 1), the L^2 gradient is computed first as an intermediate step. Identifying the Gâteaux differential (A 3) with the L^2 inner product and performing integration by parts yields

$$\nabla^{L^2}\mathcal{R}(\mathbf{u}) = \Delta(\mathbf{u} \cdot \nabla\mathbf{u}) + (\nabla\mathbf{u})^T \Delta\mathbf{u} - \mathbf{u} \cdot \nabla(\Delta\mathbf{u}) - 2\nu\Delta^2\mathbf{u}. \quad (\text{A } 5)$$

The inner product in $H^2(\Omega)$ is defined here as $\langle \mathbf{z}_1, \mathbf{z}_2 \rangle_{H^2(\Omega)} := \int_{\Omega} \mathbf{z}_1 \cdot \mathbf{z}_2 + \ell_1^2 \nabla\mathbf{z}_1 : \nabla\mathbf{z}_2 + \ell_2^4 \Delta\mathbf{z}_1 \cdot \Delta\mathbf{z}_2 \, d\mathbf{x}$, $\forall \mathbf{z}_1, \mathbf{z}_2 \in H^2(\Omega)$, where $\ell_1, \ell_2 \in \mathbb{R}_+$ are parameters with the meaning of length scales (clearly, the inner products are equivalent as long as $0 < \ell_1, \ell_2 < \infty$). Identifying the Gâteaux differential (A 3) with the H^2 inner product, integrating by parts and using (A 5), we obtain the required H^2 gradient $\nabla\mathcal{R}$ as a solution of the elliptic boundary-value problem

$$\left[\text{Id} - \ell_1^2 \Delta + \ell_2^4 \Delta^2 \right] \nabla\mathcal{R} = \nabla^{L^2}\mathcal{R} \quad \text{in } \Omega, \quad (\text{A } 6)$$

Periodic Boundary Conditions.

As shown in [79], extraction of gradients in spaces of smoother functions such as $H^2(\Omega)$ can be interpreted as low-pass filtering of the L^2 gradients with parameters ℓ_1 and ℓ_2 acting as the cut-off length-scales. The values of ℓ_1 and ℓ_2 can significantly affect the rate of convergence of the iterative procedure (A 1).

The step size τ_n in algorithm (A 1) is computed as

$$\tau_n = \operatorname{argmax}_{\tau > 0} \left\{ \mathcal{R} \left[\mathbb{P}_{\mathcal{S}_{\mathcal{E}_0}} \left(\mathbf{u}^{(n)} + \tau \nabla\mathcal{R}(\mathbf{u}^{(n)}) \right) \right] \right\} \quad (\text{A } 7)$$

which is done using a suitable derivative-free line-search algorithm [95]. Equation (A 7) can be interpreted as a modification of a standard line search method where optimization is performed following an arc (a geodesic) lying on the constraint manifold $\mathcal{S}_{\mathcal{E}_0}$, rather than a straight line.

To ensure the maximizers $\tilde{\mathbf{u}}_{\mathcal{E}_0}$ obtained for different values of \mathcal{E}_0 lie on the same maximizing branch we use a continuation approach, where the maximizer $\tilde{\mathbf{u}}_{\mathcal{E}_0}$ is employed as the initial guess \mathbf{u}^0 to compute $\tilde{\mathbf{u}}_{\mathcal{E}_0 + \Delta\mathcal{E}}$ using (A 1) at the next enstrophy level for some sufficiently small $\Delta\mathcal{E} > 0$. We refer the reader to [11] for further details and add that in their seminal study [28] Lu and Doering used the alternative ‘‘discretize-then-optimize’’ approach.

In addition to some obvious simplifications, solution of Problem 3 does involve one important complication, namely, the constraint manifold $\mathcal{W}_{\mathcal{K}_0, \mathcal{P}_0}$ is defined as an intersection of two nonlinear manifolds. As a result, the projection operator $\mathbb{P}_{\mathcal{W}_{\mathcal{K}_0, \mathcal{P}_0}}$ has a more complicated structure: while the energy constraint $\frac{1}{2} \int_{\Omega} |\nabla\psi|^2 \, d\Omega = \mathcal{K}_0$ is enforced using normalization analogous to (A 2c), the palinstrophy constraint $\frac{1}{2} \int_{\Omega} |\nabla\Delta\psi|^2 \, d\Omega = \mathcal{P}_0$ is satisfied by solving an inner optimization problem $\min_{\phi \in H^4(\Omega)} (1/2) [\mathcal{P}(\phi) - \mathcal{P}_0]^2$ subject to $\mathcal{K}(\phi) = \mathcal{K}_0$ each time the objective functional is evaluated in the discrete gradient flow (A 1).

(b) Solution of Problem 5

Local maximizers of Problem 5 are determined with an approach similar to the method described in Section (a) with one important difference, namely, the gradient $\nabla\mathcal{E}_T(\mathbf{u}_0)$ now needs to account for the flow evolution which is done using methods of the adjoint calculus [13]. Given the definition of the objective functional $\mathcal{E}_T(\mathbf{u}_0)$, its Gâteaux differential can be expressed as

$$\mathcal{E}'_T(\mathbf{u}_0; \mathbf{u}'_0) = \int_{\Omega} (\nabla \times \mathbf{u}(T, \mathbf{x})) \cdot (\nabla \times \mathbf{u}'(T, \mathbf{x})) \, d\mathbf{x} = \int_{\Omega} \Delta\mathbf{u}(T, \mathbf{x}) \cdot \mathbf{u}'(T, \mathbf{x}) \, d\mathbf{x}, \quad (\text{A } 8)$$

where the last equality follows from integration by parts and the vector identity $\nabla \times (\nabla \times \mathbf{z}) = \nabla(\nabla \cdot \mathbf{z}) - \Delta\mathbf{z}$, whereas the perturbation field $\mathbf{u}' = \mathbf{u}'(t, \mathbf{x})$ is a solution of the Navier-Stokes

system linearized around the trajectory corresponding to the initial data \mathbf{u}_0 [60], i.e.,

$$\mathcal{L} \begin{bmatrix} \mathbf{u}' \\ p' \end{bmatrix} := \begin{bmatrix} \partial_t \mathbf{u}' + \mathbf{u}' \cdot \nabla \mathbf{u} + \mathbf{u} \cdot \nabla \mathbf{u}' + \nabla p' - \nu \Delta \mathbf{u}' \\ \nabla \cdot \mathbf{u}' \end{bmatrix} = \begin{bmatrix} \mathbf{0} \\ 0 \end{bmatrix}, \quad (\text{A } 9a)$$

$$\mathbf{u}'(0) = \mathbf{u}'_0 \quad (\text{A } 9b)$$

which is subject to the periodic boundary conditions and where p' is the perturbation pressure.

We note that expression (A 8) for the Gâteaux differential is not consistent with the Riesz form (A 4), because the perturbation \mathbf{u}'_0 of the initial data does not appear in it explicitly as a factor, but is instead hidden as the initial condition in the linearized problem, cf. (A 9b). In order to transform (A 8) to the Riesz form, we introduce the *adjoint state* $\mathbf{u}^* : [0, T] \times \Omega \rightarrow \mathbb{R}^3$ and $p^* : [0, T] \times \Omega \rightarrow \mathbb{R}$, and the following duality-pairing relation

$$\begin{aligned} \left(\mathcal{L} \begin{bmatrix} \mathbf{u}' \\ p' \end{bmatrix}, \begin{bmatrix} \mathbf{u}^* \\ p^* \end{bmatrix} \right) &:= \int_0^T \int_{\Omega} \mathcal{L} \begin{bmatrix} \mathbf{u}' \\ p' \end{bmatrix} \cdot \begin{bmatrix} \mathbf{u}^* \\ p^* \end{bmatrix} dx dt = \left(\begin{bmatrix} \mathbf{u}' \\ p' \end{bmatrix}, \mathcal{L}^* \begin{bmatrix} \mathbf{u}^* \\ p^* \end{bmatrix} \right) + \\ &\quad \underbrace{\int_{\Omega} \mathbf{u}'(T, \mathbf{x}) \cdot \mathbf{u}^*(T, \mathbf{x}) dx - \int_{\Omega} \mathbf{u}'(0, \mathbf{x}) \cdot \mathbf{u}^*(0, \mathbf{x}) dx}_{\mathcal{E}'_T(\mathbf{u}_0; \mathbf{u}'_0)} = 0. \end{aligned} \quad (\text{A } 10)$$

Performing integration by parts with respect to both space and time then allows us to define the *adjoint system* as

$$\mathcal{L}^* \begin{bmatrix} \mathbf{u}^* \\ p^* \end{bmatrix} := \begin{bmatrix} -\partial_t \mathbf{u}^* - [\nabla \mathbf{u}^* + (\nabla \mathbf{u}^*)^T] \mathbf{u} - \nabla p^* - \nu \Delta \mathbf{u}^* \\ -\nabla \cdot \mathbf{u}^* \end{bmatrix} = \begin{bmatrix} \mathbf{0} \\ 0 \end{bmatrix}, \quad (\text{A } 11a)$$

$$\mathbf{u}^*(T) = \Delta \mathbf{u} \quad (\text{A } 11b)$$

which is also subject to the periodic boundary conditions. We note that in identity (A 10) all boundary terms resulting from integration by parts with respect to the space variables vanish due to the periodic boundary conditions. The term $\int_{\Omega} \mathbf{u}'(T, \mathbf{x}) \cdot \mathbf{u}^*(T, \mathbf{x}) dx$ resulting from integration by parts with respect to time is equal to the Gâteaux differential (A 8) due to the judicious choice of the terminal condition (A 11b), such that identity (A 10) implies $\mathcal{E}'_T(\mathbf{u}_0; \mathbf{u}'_0) = \int_{\Omega} \mathbf{u}'_0(\mathbf{x}) \cdot \mathbf{u}^*(0, \mathbf{x}) dx$, from which we deduce the following expression for the L^2 gradient

$$\nabla^{L^2} \mathcal{E}_T(\mathbf{u}_0) = \mathbf{u}^*(0). \quad (\text{A } 12)$$

The corresponding H^1 Sobolev gradient $\nabla \mathcal{E}_T(\mathbf{u}_0)$ is then computed as in Section (a), using the Riesz identity to obtain an elliptic boundary-value problem satisfied by the Sobolev gradient, cf. (A 4) and (A 6).

(c) Numerical Implementation

Since Problems 1–6 are all defined on periodic domains, they can be accurately discretized in space using standard Fourier pseudospectral methods with dealiasing [96,97]. For the time-dependent problems, the time discretization was performed using semi-implicit Runge-Kutta methods. For 3D Problems 4, 5 and 6 typical spatial resolutions varied from 128^3 to 512^3 gridpoints which required massively parallel implementations based on the Message Passing Interface (MPI). Solution of a single instance of Problem 5 or 6 usually required a computational time of $\mathcal{O}(10^2)$ hours on $\mathcal{O}(10^2)$ CPU cores. The reader is referred to [8,9,11,13,24] for further technical details.

Data Accessibility. This article has no additional data.

Funding. The author acknowledges the support through an NSERC (Canada) Discovery Grant. Computational resources were provided by Compute Canada under its Resource Allocation Competitions.

Acknowledgements. This work is dedicated to the memory of the late Charlie Doering, our dear friend and collaborator, who inspired us to pursue this research direction. The original plan was for this review article to

be written jointly with Charlie, but his untimely death took him before writing could begin. The author thanks the current and former members of his research group: Diego Ayala, Di Kang, Pritpal “Pip” Matharu, Diogo Poças, Elkin Ramirez, Adam Śliwiak, Dongfang Yun and Xinyu Zhao for their contributions to the research program surveyed in this paper. The author also thanks Miguel Bustamante, Sergei Chernyshenko, Giovanni Fantuzzi, David Goluskin, John Gibbon, Thomas Y. Hou, Evan Miller, Koji Ohkitani, Dmitry Pelinovsky and Tsuyoshi Yoneda for many enlightening and enjoyable discussions. The author acknowledges useful feedback provided by the referees.

References

1. Doering CR. 2009 The 3D Navier-Stokes Problem. *Annual Review of Fluid Mechanics* **41**, 109–128.
2. Robinson JC. 2020 The Navier-Stokes regularity problem. *Phil. Trans. R. Soc. A* **378**, 20190526.
3. Kreiss H, Lorenz J. 2004 *Initial-Boundary Value Problems and the Navier-Stokes Equations* vol. 47 *Classics in Applied Mathematics*. SIAM.
4. Fefferman CL. 2000 Existence and Smoothness of the Navier-Stokes Equation. available at <http://www.claymath.org/sites/default/files/navierstokes.pdf>. Clay Millennium Prize Problem Description.
5. Leray J. 1934 Sur le mouvement d’un liquide visqueux emplissant l’espace. *Acta Mathematica* **63**, 193–248.
6. Buckmaster T, Vicol V. 2019 Nonuniqueness of weak solutions to the Navier-Stokes equation. *Annals of Mathematics* **189**, 101–144.
7. Gibbon JD, Bustamante M, Kerr RM. 2008 The three-dimensional Euler equations: singular or non-singular?. *Nonlinearity* **21**, 123–129.
8. Ayala D, Protas B. 2011 On Maximum Enstrophy Growth in a Hydrodynamic System. *Physica D* **240**, 1553–1563.
9. Ayala D, Protas B. 2014a Maximum Palinstrophy Growth in 2D Incompressible Flows. *Journal of Fluid Mechanics* **742**, 340–367.
10. Ayala D, Protas B. 2014b Vortices, maximum growth and the problem of finite-time singularity formation. *Fluid Dynamics Research* **46**, 031404.
11. Ayala D, Protas B. 2017 Extreme Vortex States and the Growth of Enstrophy in 3D Incompressible Flows. *Journal of Fluid Mechanics* **818**, 772–806.
12. Yun D, Protas B. 2018 Maximum Rate of Growth of Enstrophy in Solutions of the Fractional Burgers Equation. *Journal of Nonlinear Science* **28**, 395–422.
13. Kang D, Yun D, Protas B. 2020 Maximum amplification of enstrophy in three-dimensional Navier-Stokes flows. *Journal of Fluid Mechanics* **893**, A22.
14. Adams RA, Fournier JF. 2005 *Sobolev Spaces*. Elsevier.
15. Robinson JC, Rodrigo JL, Sadowski W. 2016 *The Three-Dimensional Navier-Stokes Equations: Classical Theory*. Cambridge University Press.
16. Foias C, Temam R. 1989 Gevrey Class Regularity for the Solutions of the Navier-Stokes Equations. *Journal of Functional Analysis* **87**, 359–369.
17. Kiselev AA, Ladyzhenskaya OA. 1957 On the existence and uniqueness of the solution of the nonstationary problem for a viscous, incompressible fluid. *Izv. Akad. Nauk SSSR Ser. Mat* **21**, 655–680.
18. Prodi G. 1959 Un teorema di unicità per le equazioni di Navier-Stokes. *Annali di Matematica Pura ed Applicata* **48**, 173–182.
19. Serrin J. 1962 On the interior regularity of weak solutions of the Navier-Stokes equations. *Archive for Rational Mechanics and Analysis* **9**, 187–195.
20. Gibbon JD. 2018 Weak and Strong Solutions of the 3D Navier-Stokes Equations and Their Relation to a Chessboard of Convergent Inverse Length Scales. *Journal of Nonlinear Science*. (published on-line).
21. Escauriaza L, Seregin GA, Sverak V. 2003 $L^{3,\infty}$ -solutions of the Navier-Stokes equations and backward uniqueness. *Russian Mathematical Surveys* **58**, 211–250.
22. Tao T. 2020 Quantitative bounds for critically bounded solutions to the Navier-Stokes equations. arXiv:1908.04958.
23. Constantin P. 1991 Remarks on the Navier-Stokes equations. In Sirovich L, editor, *New Perspectives in Turbulence* pp. 229–261. Berlin: Springer.

24. Kang D, Protas B. 2021 Searching for Singularities in Navier-Stokes Flows Based on the Ladyzhenskaya-Prodi-Serrin Conditions. arXiv:2110.06130.
25. Beale JT, Kato T, Majda A. 1984 Remarks on the breakdown of smooth solutions for the 3-D Euler equations. *Comm. Math. Phys.* **94**, 61–66.
26. Constantin P. 1986 Note on loss of regularity for solutions of the 3—D incompressible euler and related equations. *Communications in Mathematical Physics* **104**, 311–326.
27. Elgindi TM, Jeong IJ. 2019 Finite-Time Singularity Formation for Strong Solutions to the Axisymmetric 3D Euler Equations. *Annals of PDE* **5**, 16.
28. Lu L, Doering CR. 2008 Limits on Enstrophy Growth for Solutions of the Three-dimensional Navier–Stokes Equations. *Indiana University Mathematics Journal* **57**, 2693–2727.
29. Giga Y. 1986 Solutions for semilinear parabolic equations in L^p and regularity of weak solutions of the Navier-Stokes system. *Journal of Differential Equations* **62**, 186–212.
30. Robinson JC, Sadowski W, Silva RP. 2012 Lower bounds on blow up solutions of the three-dimensional Navier Stokes equations in homogeneous Sobolev spaces. *Journal of Mathematical Physics* **53**, 115618.
31. Robinson JC, Sadowski W. 2014 A local smoothness criterion for solutions of the 3D Navier-Stokes equations. *Rendiconti del Seminario Matematico della Università di Padova* **131**, 159–178.
32. Brachet ME, Meiron DI, Orszag SA, Nickel BG, Morf RH, Frisch U. 1983 Small-scale Structure of the Taylor–Green Vortex. *Journal of Fluid Mechanics* **130**, 411–452.
33. Pumir A, Siggia E. 1990 Collapsing solutions to the 3D Euler equations. *Phys. Fluids A* **2**, 220–241.
34. Brachet ME. 1991 Direct Simulation of Three-dimensional Turbulence in the Taylor-Green Vortex. *Fluid Dynamics Research* **8**, 1–8.
35. Kerr RM. 1993 Evidence for a Singularity of the Three-dimensional, Incompressible Euler Equations. *Phys. Fluids A* **5**, 1725–1746.
36. Pelz RB. 2001 Symmetry and the hydrodynamic blow-up problem. *Journal of Fluid Mechanics* **444**, 299–320.
37. Bustamante MD, Kerr RM. 2008 3D Euler about a 2D symmetry plane. *Physica D* **237**, 1912–1920.
38. Ohkitani K, Constantin P. 2008 Numerical study of the Eulerian–Lagrangian analysis of the Navier-Stokes turbulence. *Phys. Fluids* **20**, 1–11.
39. Ohkitani K. 2008 A miscellany of basic issues on incompressible fluid equations. *Nonlinearity* **21**, 255–271.
40. Grafke T, Homann H, Dreher J, Grauer R. 2008 Numerical simulations of possible finite-time singularities in the incompressible Euler equations: comparison of numerical methods. *Physica D* **237**, 1932–1936.
41. Hou TY. 2009 Blow-up or No Blow-up? A Unified Computational and Analytic Approach to 3D Incompressible Euler and Navier–Stokes Equations. *Acta Numerica* pp. 277–346.
42. Orlandi P, Pirozzoli S, Carnevale GF. 2012 Vortex events in Euler and Navier-Stokes simulations with smooth initial conditions. *Journal of Fluid Mechanics* **690**, 288–320.
43. Bustamante MD, Brachet M. 2012 Interplay between the Beale-Kato-Majda theorem and the analyticity-strip method to investigate numerically the incompressible Euler singularity problem. *Phys. Rev. E* **86**, 066302.
44. Orlandi P, Pirozzoli S, Bernardini M, Carnevale GF. 2014 A minimal flow unit for the study of turbulence with passive scalars. *Journal of Turbulence* **15**, 731–751.
45. Campolina CS, Mailybaev AA. 2018 Chaotic Blowup in the 3D Incompressible Euler Equations on a Logarithmic Lattice. *Phys. Rev. Lett.* **121**, 064501.
46. Donzis DA, Gibbon JD, Gupta A, Kerr RM, Pandit R, Vincenzi D. 2013 Vorticity moments in four numerical simulations of the 3D Navier-Stokes equations. *Journal of Fluid Mechanics* **732**, 316–331.
47. Kerr RM. 2013 Swirling, turbulent vortex rings formed from a chain reaction of reconnection events. *Physics of Fluids* **25**, 065101.
48. Gibbon J, Donzis D, Gupta A, Kerr R, Pandit R, Vincenzi D. 2014 Regimes of nonlinear depletion and regularity in the 3D Navier-Stokes equations. *Nonlinearity* **27**.
49. Kerr RM. 2013 Bounds for Euler from vorticity moments and line divergence. *Journal of Fluid Mechanics* **729**, R2.
50. Kerr RM. 2018 Enstrophy and circulation scaling for Navier-Stokes reconnection. *Journal of Fluid Mechanics* **839**, R2.

51. Moffatt HK, Kimura Y. 2019a Towards a finite-time singularity of the Navier-Stokes equations Part 1. Derivation and analysis of dynamical system. *Journal of Fluid Mechanics* **861**, 930–967.
52. Moffatt HK, Kimura Y. 2019b Towards a finite-time singularity of the Navier-Stokes equations. Part 2. Vortex reconnection and singularity evasion. *Journal of Fluid Mechanics* **870**, R1.
53. Matsumoto T, Bec J, Frisch U. 2008 Complex-space singularities of 2D Euler flow in Lagrangian coordinates. *Physica D* **237**, 1951–1955.
54. Siegel M, Caflisch RE. 2009 Calculation of complex singular solutions to the 3D incompressible Euler equations. *Physica D* **238**, 2368–2379.
55. Luo G, Hou TY. 2014a Potentially Singular Solutions of the 3D Axisymmetric Euler Equations. *Proceedings of the National Academy of Sciences* **111**, 12968–12973.
56. Luo G, Hou TY. 2014b Toward the Finite-Time Blowup of the 3D Incompressible Euler Equations: a Numerical Investigation. *SIAM: Multiscale Modeling and Simulation* **12**, 1722–1776.
57. Hou TY, Huang D. 2021 Potential Singularity Formation of 3D Axisymmetric Navier-Stokes Equations with Degenerate Diffusion Coefficients. arXiv:2102.06663.
58. Abergel F, Temam R. 1990 On Some Control Problems in Fluid Mechanics. *Theoretical and Computational Fluid Dynamics* **1**, 303–325.
59. Fursikov AV. 2000 *Optimal Control of Distributed Systems. Theory and Applications*. Translations of Mathematical Monographs. American Mathematical Society.
60. Gunzburger MD. 2003 *Perspectives in Flow Control and Optimization*. SIAM.
61. Tröltzsch F. 2010 *Optimal Control of Partial Differential Equations: Theory, Methods and Applications* vol. 112 *Graduate Studies in Mathematics*. American Mathematical Society.
62. Bec J, Khanin K. 2007 Burgers turbulence. *Physics Reports* **447**, 1–66.
63. Biryuk AÈ. 2001 Spectral Properties of Solutions of the Burgers Equation with Small Dissipation. *Functional Analysis and Its Applications* **35**, 1–12.
64. Pelinovsky D. 2012a Sharp bounds on enstrophy growth in the viscous Burgers equation. *Proceedings of Royal Society A* **468**, 3636–3648.
65. Pelinovsky D. 2012b Enstrophy growth in the viscous Burgers equation. *Dynamics of Partial Differential Equations* **9**, 305–340.
66. Fantuzzi G, Goluskin D. 2020 Bounding Extreme Events in Nonlinear Dynamics Using Convex Optimization. *SIAM Journal on Applied Dynamical Systems* **19**, 1823–1864.
67. Flandoli F. 2015 *Random Perturbation of PDEs and Fluid Dynamic Models*. Lecture Notes in Mathematics. Springer.
68. Poças D, Protas B. 2018 Transient growth in stochastic Burgers flows. *Discrete & Continuous Dynamical Systems — B* **23**, 2371.
69. Kiselev A, Nazaraov F, Shterenberg R. 2008 Blow up and regularity for fractal Burgers equation. *Dynamics of Partial Differential Equations* **5**, 211–240.
70. Katz N, Pavlović N. 2002 A cheap Caffarelli-Kohn-Nirenberg inequality for the Navier-Stokes equation with hyper-dissipation. *Geometric & Functional Analysis GFA* **12**, 355–379.
71. Boritchev A. 2018 Decaying turbulence for the fractional subcritical Burgers equation. *Discrete & Continuous Dynamical Systems* **38**, 2229–2249.
72. Ramírez E, Protas B. 2021 Singularity Formation in the Deterministic and Stochastic Fractional Burgers Equation. arXiv:2104.10759.
73. Ayala D, Doering CR, Simon TM. 2018 Maximum palinstrophy amplification in the two-dimensional Navier-Stokes equations. *Journal of Fluid Mechanics* **837**, 839–857.
74. Tran CV, Dritschel DG. 2006 Vanishing enstrophy dissipation in two-dimensional Navier-Stokes turbulence in the inviscid limit. *Journal of Fluid Mechanics* **559**, 107–116.
75. Dascaluic R, Foias C, Jolly MS. 2010 Estimates on enstrophy, palinstrophy, and invariant measures for 2D turbulence. *Journal of Differential Equations* **248**, 792–819.
76. Jeong IJ, Yoneda T. 2021 Enstrophy dissipation and vortex thinning for the incompressible 2D Navier-Stokes equations. *Nonlinearity* **34**, 1837–1853.
77. Śliwiak A. 2017 Maximum Rate of Growth of Enstrophy in the Navier-Stokes System on 2D Bounded Domains. Master's thesis McMaster University.
78. Taylor GI, Green AE. 1937 Mechanism of the production of small eddies from large ones. *Proceedings of the Royal Society of London A* **158**, 499–521.
79. Protas B, Bewley T, Hagen G. 2004 A comprehensive framework for the regularization of adjoint analysis in multiscale PDE systems. *Journal of Computational Physics* **195**, 49–89.
80. Protas B. 2008 Adjoint-Based optimization of PDE systems with alternative gradients. *Journal of Computational Physics* **227**, 6490–6510.

81. Luenberger D. 1969 *Optimization by Vector Space Methods*. John Wiley and Sons.
82. Huang D, Chernyshenko S, Goulart P, Lasagna D, Tutty O, Fuentes F. 2015 Sum-of-squares of polynomials approach to nonlinear stability of fluid flows: an example of application. *Proceedings of the Royal Society of London. Series A, Mathematical and physical sciences* **471**, 1–18.
83. Lasagna D, Huang D, Tutty O, Chernyshenko S. 2016 Sum-of-Squares approach to feedback control of laminar wake flows. *Journal of Fluid Mechanics* **809**, 628–663.
84. Fantuzzi G, Goluskin D, Huang D, Chernyshenko SI. 2016 Bounds for Deterministic and Stochastic Dynamical Systems using Sum-of-Squares Optimization. *SIAM Journal on Applied Dynamical Systems* **15**, 1962–1988.
85. Goluskin D. 2018 Bounding Averages Rigorously Using Semidefinite Programming: Mean Moments of the Lorenz System. *Journal of Nonlinear Science* **28**, 621–651.
86. Tobasco I, Goluskin D, Doering CR. 2018 Optimal bounds and extremal trajectories for time averages in nonlinear dynamical systems. *Physics Letters A* **382**, 382–386.
87. Doering CR, Constantin P. 1992 Energy dissipation in shear driven turbulence. *Phys. Rev. Lett.* **69**, 1648–1651.
88. Fantuzzi G, Arslan A, Wynn A. 2021 The background method: Theory and computations. arXiv:2107.11206.
89. Jameson A. 1988 Aerodynamic design via control theory. *Journal of Scientific Computing* **3**, 233–260.
90. Kim N. 2003 Remarks for the axisymmetric Navier-Stokes equations. *Journal of Differential Equations* **187**, 226–239.
91. Eggl MF, Schmid PJ. 2020 Mixing enhancement in binary fluids using optimised stirring strategies. *Journal of Fluid Mechanics* **899**, A24.
92. Miles CJ, Doering CR. 2018 A Shell Model for Optimal Mixing. *Journal of Nonlinear Science* **28**, 2153–2186.
93. Rabin SME, Caulfield CP, Kerswell RR. 2012 Variational identification of minimal seeds to trigger transition in plane Couette flow. *Journal of Fluid Mechanics* **712**, 244–272.
94. Grafke T, Grauer R, Schäfer T. 2015 The instanton method and its numerical implementation in fluid mechanics. *Journal of Physics A: Mathematical and Theoretical* **48**, 333001.
95. Ruszczyński A. 2006 *Nonlinear Optimization*. Princeton University Press.
96. Boyd JP. 2001 *Chebyshev and Fourier Spectral Methods*. Dover.
97. Canuto C, Quarteroni A, Hussaini Y, Zang TA. 2006 *Spectral Methods*. Scientific Computation. Springer.